The Joint Impacts of Atlantic and Pacific Multidecadal Variability on South American Precipitation and Temperature

ZHAOXIANGRUI HE,[a] AIGUO DAI,[a] AND MATHIAS VUILLE[a]

[a] *Department of Atmospheric and Environmental Sciences, University at Albany, State University of New York, Albany, New York*

(Manuscript received 28 January 2021, in final form 5 July 2021)

ABSTRACT: South American climate is influenced by both Atlantic multidecadal variability (AMV) and Pacific multidecadal variability (PMV). But how they jointly affect South American precipitation and surface air temperature is not well understood. Here we analyze composite anomalies to quantify their combined impacts using observations and reanalysis data. During an AMV warm (cold) phase, PMV-induced JJA precipitation anomalies are more positive (negative) over 0°–10°S and southeastern South America, but more negative (positive) over the northern Amazon and central Brazil. PMV-induced precipitation anomalies in DJF are more positive (negative) over northeast Brazil and southeastern South America during the warm (cold) AMV phase, but more negative (positive) over the central Amazon basin and central-eastern Brazil. PMV's impact on AMV-induced precipitation anomalies shows similar dipole patterns. The precipitation changes result from perturbations of the local Hadley and Walker circulations. In JJA, PMV- and AMV-induced temperature anomalies are more positive (negative) over the entirety of South America when the other basin is in a warm (cold) phase, but in DJF, temperature anomalies are more positive (negative) only over the central Andes and central-eastern Brazil and more negative (positive) over southeastern South America and Patagonia. Over central Brazil in JJA and southern Bolivia and northern Argentina in DJF, the temperature and precipitation anomalies are negatively correlated. Our results show that the influence of Pacific and Atlantic multidecadal variability needs to be considered jointly, as significant departures from the mean AMV or PMV fingerprint can occur during a cold or warm phase of the other basin's mode.

KEYWORDS: Atmosphere; Ocean; Atlantic Ocean; Pacific Ocean; South America; Hadley circulation; Walker circulation; Precipitation; Climate variability; Multidecadal variability

1. Introduction

The climate of South America varies from intraseasonal and seasonal to interannual, decadal, and multidecadal time scales. On seasonal time scales, the intertropical convergence zone (ITCZ) migrates southward over both the Pacific and Atlantic during the austral summer [December–January–February (DJF)], resulting in rainfall over coastal Ecuador and a few months later, in March–May, also over Northeastern Brazil. Over the South American continent, atmospheric convective activity extends from the southern half of the Amazon basin to northern Argentina and over the subtropical South Atlantic, associated with the buildup of the South American summer monsoon (SASM) and the South Atlantic convergence zone (SACZ), respectively (Garreaud et al. 2009). The SASM starts to develop by the end of October and reaches its demise by April of the following year. Diabatic heating over the Amazon basin associated with local precipitation is conducive for the formation of the Bolivian high (Lenters and Cook 1997), which facilitates easterly moisture transport from the Amazon basin to the Central Andes and northern Altiplano (Garreaud et al. 2003). The SACZ on the other hand, exists all year-round, but is more strongly developed during austral summer. It is characterized by an elongated band of convective cloudiness and precipitation that extends from the Amazon basin to the subtropical South Atlantic in a northwest–southeast direction, fed by moisture transported by low-level winds from the Amazon basin to southeastern Brazil (Carvalho et al. 2004), and formed by Rossby wave train propagation (Liebmann et al. 1999). During the austral winter [June–July–August (JJA)], the Atlantic ITCZ migrates northward and the convective activity withdraws to northern South America (north of ~5°S), which brings abundant precipitation to northernmost South America north of the equator.

While this seasonal cycle and its hydroclimatic impacts over South America are generally well established, much less is known about how internal variability, especially on decadal or multidecadal time scales, modifies this seasonality and thereby perturbs the temperature and precipitation signal over South America. Internal variability results from ocean–atmosphere interactions over the Pacific and Atlantic oceans, such as the influence of El Niño–Southern Oscillation (ENSO) (Cai et al. 2020). A better understanding of internal variability and its role in modifying the seasonal cycle over South America is also helpful for projecting future changes in climate, because internal variability is superimposed on any global warming trend and thereby slows or accelerates this trend. While ENSO's role in driving interannual climate variability over South America is reasonably well understood (Sulca et al. 2018; Cai et al. 2020), much less is known about how modes of decadal and multidecadal variability affect this region. This lack of understanding is to a large extent driven by the rather short records of observations from both South America and the two neighboring ocean basins (Garreaud et al. 2009), which hampers analysis of multidecadal variability.

The Pacific multidecadal variability (PMV; Liu 2012), also known as the interdecadal Pacific oscillation (Power et al. 1999)

Corresponding author: Mathias Vuille, mvuille@albany.edu

DOI: 10.1175/JCLI-D-21-0081.1

or Pacific decadal oscillation for its North Pacific component (Zhang et al. 1997), is a multidecadal (50–70 yr) mode of variability in Pacific sea surface temperatures (SST) with spatial patterns broadly similar to ENSO but with subtle differences (e.g., larger SST anomalies off the equatorial Pacific than ENSO, Zhang et al. 1997; Dong et al. 2018). Hereafter the interdecadal Pacific oscillation and Pacific decadal oscillation will be referred to as the PMV throughout the paper. The PMV of the last 100 years or so has been attributed primarily to internal variability, although external forcing did modulate the decadal SST variations in the Pacific, especially since the early 1990s (Hua et al. 2018). Through interactions with the atmosphere, the PMV affects precipitation, temperature, and other fields (Dong and Dai 2017) over other ocean basins (Dong et al. 2016) and many land areas in Australia, India, North America, southern and West Africa, and South America (Power et al. 1999; Krishnan and Sugi 2003; Deser et al. 2004; Hartmann and Wendler 2005; Garreaud et al. 2009; Dai 2013; Dong and Dai 2015). The PMV's impacts on South American precipitation and temperature have been reported to be similar to ENSO's impacts, albeit with a much weaker amplitude (Garreaud and Battisti 1999; Garreaud et al. 2009; Flantua et al. 2016). Some studies (e.g., Garreaud et al. 2009; Dai 2013; Dong and Dai 2015, 2017; Flantua et al. 2016) have shown negative correlations with the PMV indices for precipitation over most of northern South America north of 10°S (except over the northern Amazon basin and coast of Ecuador), and positive correlations over central-eastern Brazil, eastern Bolivia, northern Argentina, and southeastern South America. Villamayor et al. (2018) showed consistent PMV precipitation patterns over northern South America in simulations of the Coupled Model Intercomparison Project Phase 5 (CMIP5). Observations also show that the PMV indices are positively correlated with temperature over the Andes, with large temperature anomalies over the central Andes. While Garreaud et al. (2009) and Flantua et al. (2016) reported positive correlations between the PMV indices and annual surface air temperature over northernmost and northeastern South America, Dong and Dai (2015) showed negative correlations over this region. The PMV SST pattern influences South American rainfall through stationary Rossby wave trains that propagate from the South Pacific Ocean to South America, i.e., the Pacific–South American (PSA) pattern (Karoly 1989; Mo and Paegle 2001). The PMV's phase transition from cold to warm in 1970s might have led to a shift in South American climate, affecting temperature and precipitation (Jacques-Coper and Garreaud 2015, Kayano et al. 2009), shortening of the SASM season (Arias et al. 2015), lengthening of the dry season in the southern Amazon (Agudelo et al. 2019), a southward shift of the SACZ (Zilli et al. 2019), increasing South American low-level jet (SALLJ) occurrences to the east of the northern Andes (Jones 2019), and increasing the variability and frequency of central Brazilian summer precipitation (Prado et al. 2021). During the recent global warming hiatus from 1999 to 2014, the cold phase of the PMV did not only slow down the global warming rate with significant cooling along the Pacific coast of South America (Vuille et al. 2015) and other parts of the world (Dai et al. 2015), but also strengthened the Pacific Walker circulation (England et al. 2014) and hence increased the frequency of extreme floods in the Amazon basin (Barichivich et al. 2018).

The Atlantic multidecadal variability (AMV; Liu 2012; Sutton et al. 2018; Zhang et al. 2019) in Atlantic SSTs, also known as the Atlantic multidecadal oscillation (Folland et al. 1984; Schlesinger and Ramankutty 1994), has significant impacts on multidecadal climate variations over North America (Ruprich-Robert et al. 2018) and Eurasia (Sutton and Dong 2012; O'Reilly et al. 2017; Luo et al. 2017), as well as Sahelian and South American rainfall (Knight et al. 2006; Hua et al. 2019), Atlantic hurricane activity (Zhang and Delworth 2006), Arctic sea ice extent (Day et al. 2012; Miles et al. 2014), and global mean temperature (Chylek et al. 2014; Dai et al. 2015). Hereafter we will refer to the Atlantic multidecadal oscillation as the AMV throughout this paper. While the AMV is thought to be an internally generated quasi-oscillation related to the Atlantic meridional overturning circulation (Zhang et al. 2019) and North Atlantic Oscillation (Sutton et al. 2018), its recent cycles have been partly attributed to in-phase external forcing from decadal variations in volcanic and anthropogenic aerosols (Qin et al. 2020a), which may also have caused AMV-like SST variations in the Pacific and other oceans (Qin et al. 2020b). Knight et al. (2006) and Flantua et al. (2016) showed that the AMV index is positively correlated with precipitation over the western and northern Amazon basin, and negatively correlated with precipitation over northeastern South America, Brazil between 10°S and 0°, and the coasts of Colombia and Ecuador. Villamayor et al. (2018) showed similar rainfall patterns over northern South America in the CMIP5 models. Flantua et al. (2016) also showed that the AMV index positively correlates with temperature over most of tropical and subtropical South America. During the AMV warm phase, the tropical North Atlantic and Caribbean Sea feature warmer than normal SST, which displaces the Atlantic ITCZ northward and weakens the SASM (Bird et al. 2011; Vuille et al. 2012; Rojas et al. 2016). This change in atmospheric circulation reduces precipitation over the southern Amazon basin and northeast Brazil, while it enhances rainfall over the northwestern Amazon basin (Hastenrath and Heller 1977; Nobre and Shukla 1996; Flantua et al. 2016; Hua et al. 2019). Several studies (Malhi et al. 2008; Marengo et al. 2008; Zeng et al. 2008) also showed that the warming of the tropical North Atlantic and hence the intensification of the tropical Atlantic meridional SST gradient can enhance the duration and intensity of the dry season in the Amazon basin, which is considered to have contributed to the 2005 Amazon drought. Surface temperature over tropical South America is also above normal when the AMV is in its warm phase, especially over the southern central Amazon basin (Flantua et al. 2016).

Our understanding of how the PMV and AMV affect South American climate is hampered not only by the limited length of observational records (Garreaud et al. 2009), but also by the fact that these modes are not independent from each other, as they can occur simultaneously (Huang et al. 2019) or interact with each other (Cai et al. 2019) and thus can jointly exert influences over South America. Therefore, a thorough analysis of their impacts on South American climate cannot be achieved

TABLE 1. The names, sources, periods, time steps, and resolutions for the datasets used in this study. See table footnotes for links to the datasets for each source.

Name	Source	Period	Time step	Resolution
HadISST	Met Office Hadley Center[a]	1920–2019	Monthly	1° × 1°
HadSST3	Met Office Hadley Center	1920–2019	Monthly	5° × 5°
ERSSTv5	National Oceanic and Atmospheric Administration (NOAA)[b]	1920–2019	Monthly	2° × 2°
Kaplan	International Research Institute for Climate and Society (IRI)[c]	1920–2019	Monthly	5° × 5°
COBE	Japan Meteorological Agency (JMA)[d]	1920–2019	Monthly	1° × 1°
CRU TS	Climatic Research Unit (CRU)[e]	1920–2017	Monthly	0.5° × 0.5°
UDelaware	University of Delaware[f]	1920–2017	Monthly	0.5° × 0.5°
GISTEMP	NASA Goddard Institute for Space Studies (GISS)[g]	1920–2017	Monthly	2° × 2°
GPCC	Global Precipitation Climatology Centre (GPCC)[h]	1920–2016	Monthly	0.5° × 0.5°
20CRv3	NOAA/Earth System Research Laboratory (ESRL), Cooperative Institute for Research in Environmental Sciences (CIRES)[i]	1920–2015	Monthly	1° × 1°
ERA5	Copernicus Climate Change Service (C3S) Climate Data Store (CDS)[j]	1950–2019	Monthly	0.25° × 0.25°

[a] https://www.metoffice.gov.uk/hadobs/hadisst/data/download.html.
[b] https://www.ncdc.noaa.gov/data-access/marineocean-data/extended-reconstructed-sea-surface-temperature-ersst-v5.
[c] http://iridl.ldeo.columbia.edu/SOURCES/.KAPLAN/.EXTENDED/.v2/.ssta/.
[d] http://ds.data.jma.go.jp/tcc/tcc/products/elnino/cobesst/cobe-sst.html.
[e] https://crudata.uea.ac.uk/cru/data/hrg/cru_ts_4.04/.
[f] http://climate.geog.udel.edu/~climate/html_pages/download.html#T2011.
[g] https://data.giss.nasa.gov/gistemp/.
[h] https://www.dwd.de/EN/ourservices/gpcc/gpcc.html.
[i] https://psl.noaa.gov/data/gridded/data.20thC_ReanV3.html.
[j] https://doi.org/10.24381/cds.6860a573.

by only considering each mode in isolation (which was the case in most previous studies), but also needs to take into account how they may mutually reinforce or dampen the influence from one another and how such interactions affect the climate over South America. There are some recent studies which have investigated how interannual and multidecadal variability of the Atlantic modulates the impacts of ENSO on South American precipitation (Kayano et al. 2011, 2013; Kayano and Capistrano 2014; Figliuolo et al. 2020). For example, Kayano et al. (2011) showed that precipitation anomalies over northeastern and southeastern South America associated with El Niño (La Niña) will change when the El Niño (La Niña) event is preceded by a cold (warm)-phase Atlantic equatorial mode. Kayano and Capistrano (2014) and Figliuolo et al. (2020) showed that rainfall over northeast Brazil and the Amazon basin associated with the eastern Pacific El Niño depends on the phase of the AMV. Kayano et al. (2019, 2020) also showed that the El Niño and La Niña's effects on South American precipitation depend on the PMV and AMV phase combinations. Furthermore, Chen et al. (2011) showed that El Niño and the warm phase of the AMV combined to cause high levels of fire activity in the southeastern and southwestern Amazon basin in 2005 and 2010, while La Niña and the cold phase of the AMV jointly led to fewer wildfires over these regions in 2001 and 2009.

While these studies have allowed us to make some progress related to joint influences from the Atlantic and the Pacific on South American climate, they did not consider how the PMV modulates the influence from the AMV (or vice versa) on South American precipitation on multidecadal time scales. Furthermore, no studies have assessed how the mutual modulations of the two ocean basins influence South American surface air temperature.

Here, we attempt to quantify the joint impacts from the PMV and AMV on South American climate by analyzing the anomaly composites of precipitation, near-surface air temperature (Tas), and atmospheric circulation under different combinations of the AMV and PMV phases using observations and reanalysis data. Because most of South America experiences a strong precipitation seasonality, and precipitation anomalies may influence Tas, we analyze both precipitation and Tas anomalies separately for austral summer (DJF) and winter (JJA).

The next section describes the datasets used, including SST, precipitation, Tas, and reanalysis data, as well as the methods used to calculate the PMV and AMV indices and to perform the composite analysis. Sections 3 and 4 present the results for South American precipitation and temperature, respectively. Section 5 summarizes the main results and ends with a discussion of the main conclusions from this study.

2. Data and methods

a. Datasets

In this study, we used datasets of SST, Tas, precipitation, and atmospheric reanalysis. The details of the datasets are summarized in Table 1. Specifically, we used monthly SST data from 1920 to 2019 obtained from five datasets, including the Hadley Centre Sea Ice and Sea Surface Temperature version 1.1 (HadISST) (Rayner et al. 2003), the Hadley Centre SST

dataset (HadSST3) (Kennedy et al. 2011a,b), the extended reconstructed sea surface temperature, version 5 (ERSSTv5) (Huang et al. 2017), the Kaplan Extended SST v2 (Kaplan) (Kaplan et al. 1998), and the Centennial In situ Observation-Based Estimates (COBE) (Ishii et al. 2005). These SST products were derived from marine observations of SSTs with varying techniques and efforts to homogenize the records.

To investigate the temperature response over South America to joint PMV/AMV variability, we used three Tas monthly datasets, including the Climatic Research Unit Time Series version 4.04 (CRU TS) 2-m temperature (Harris et al. 2020), the University of Delaware V5.01 (UDelaware) terrestrial temperature (Matsuura and Willmott 2018a), and NASA's Goddard Institute Surface Temperature version 4 (GISTEMP) temperature anomalies (Lenssen et al. 2019; GISTEMP Team 2020).

The influence of PMV/AMV variability on South American precipitation was analyzed by means of three different products, including the Global Precipitation Climatology Centre version 2018 (GPCC) precipitation (Schneider et al. 2018), the CRU TS precipitation (Harris et al. 2020), and the UDelaware terrestrial precipitation (Matsuura and Willmott 2018b). These land Tas and precipitation products were derived from weather station observations, which are sparse over the Amazon basin, southern Brazil, and the central and southernmost Andes Mountains; thus, results over these regions may be less reliable. On the other hand, there are more stations and longer records available along the coastlines (Garreaud et al. 2009).

Finally, we used monthly atmospheric reanalysis data for upper-air fields from the twentieth century Reanalysis V3 (20CRv3, Slivinski et al. 2019) and the fifth-generation European Centre for Medium-Range Weather Forecasts reanalysis (ERA5; Hersbach et al. 2019; Bell et al. 2020).

b. *Pacific multidecadal index*

We defined a PMV index as the 11-yr moving averaged tripole index (TPI), which was proposed by Henley et al. (2015). The TPI is defined as follows:

$$\mathrm{TPI} = \mathrm{SSTA}_2 - \frac{\mathrm{SSTA}_1 + \mathrm{SSTA}_3}{2}, \tag{1}$$

where the SSTA_i (i = 1, 2, 3) are the (annual and seasonal) linearly detrended SST anomalies (relative to the 1920–2015 mean) averaged over each of the three TPI regions: i = 1 for the northwestern Pacific (25°–45°N, 140°E–145°W), i = 2 for the equatorial central to eastern Pacific (10°S–10°N, 170°E–90°W), and i = 3 for the southwestern Pacific (50°–15°S, 150°E–160°W). We used the 11-yr moving average of the TPI to isolate the decadal-to-longer time scale variability of the PMV from the variability of higher frequency. The 11-yr moving average was applied to the time series with mirrored end points. The PMV indices calculated from the HadSST3, ERSSTv5, Kaplan, and COBE datasets are consistent with one another (Fig. 1a), and they are also consistent with Henley et al. (2015) and Hua et al. (2018). While the linear detrending removes most of the anthropogenic warming signal, decadal variations in external forcing may still contribute noticeably to the TPI or its smoothed version (i.e., the PMV index), mainly since the early 1990s (Hua et al. 2018).

c. *Atlantic multidecadal index*

By definition, an oscillation represents deviations relative to a stable mean or a long-term trend. Therefore, we followed Enfield et al. (2001) to define an AMV index from 1920 to 2019 as the 11-yr moving average of the (annual and seasonal) linearly detrended SST anomalies (relative to the 1920–2015 mean) averaged over the North Atlantic (0°–60°N, 0°–80°W) with mirrored data near the last end point. The AMV indices calculated using the HadSST3, ERSSTv5, Kaplan, and COBE products are all consistent with one another (Fig. 1b), and in agreement with Ting et al. (2009) and Ruprich-Robert et al. (2017). However, the AMV index may differ considerably if the detrending is done over different time periods or if other methods were used to remove the long-term changes (Qin et al. 2020a,b).

We also employ the Atlantic north–south SST gradient (ANSG) to quantify the meridional SST gradient over the tropical Atlantic following Hua et al. (2019). The ANSG is defined as the 11-yr moving average of the (annual and seasonal) linearly detrended SST difference between the tropical North (15°–75°W and 5°–30°N) and South (40°W–20°E and 5°–30°S) Atlantic. A positive ANSG index implies an anomalously warm tropical North Atlantic relative to the tropical South Atlantic.

d. *Composite analysis*

To focus on multidecadal variations, before computing composite anomalies, we converted all the seasonal data series into anomalies relative to a reference period from 1920 to 2015 (over which both the AMV and PMV indices (Fig. 1) have a near-zero mean), linearly detrended them, and smoothed them using an 11-yr running mean (with mirrored data near the last end point). Unlike linear regression, our composite analysis does not assume linearity among the effects from the AMV and PMV.

We employ composite analysis to investigate the 11-yr smoothed temperature, precipitation and atmospheric circulation anomalies associated with the different phase combinations of the (11-yr smoothed) AMV and PMV. We first group all years into three categories, based on the value of the AMV index in that particular year. We use "P" and "A" to represent the PMV and AMV, respectively, and "w," "n," and "c" to represent the warm, neutral, and cold phase of the PMV and AMV, following Schubert et al. (2009). Years when the AMV index $> 0.5\sigma$ (σ = standard deviation) are grouped into the warm AMV (Aw) ensemble; years when the AMV index $< -0.5\sigma$ are grouped into the cold AMV (Ac) ensemble, and all other years fall into the neutral AMV (An) ensemble. Similarly, years with warm, cold and neutral PMV phases (Pw, Pc, and Pn, respectively) are clustered. Then, following Huang et al. (2019), the years are grouped according to the nine possible AMV/PMV phase combinations resulting in nine different clusters, shown in Fig. 1c, used to calculate the composites. As an example, the "PwAc" composite stands for the average of the subset of years with a simultaneous warm phase of the PMV (Pw) and a cold phase of the AMV (Ac). This approach is

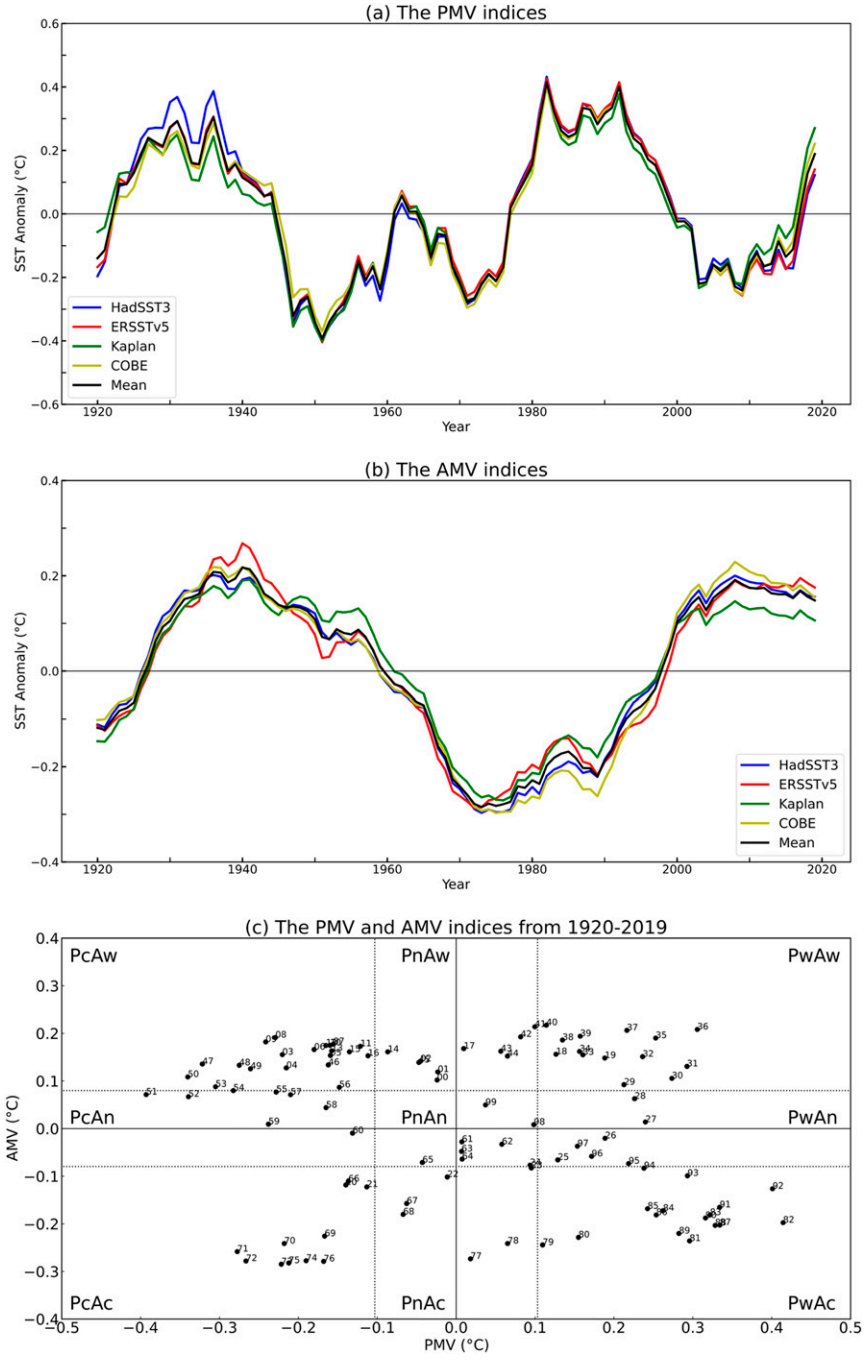

FIG. 1. The times series of the annual (a) PMV indices and (b) AMV indices from 1920 to 2019 from the HadSST3, ERSSTv5, Kaplan, and COBE datasets. The black lines show the means of the PMV and AMV indices based on the four datasets. Mirrored data points were used near the last end point. (c) The scatterplot of the PMV and AMV indices, based on the mean of the four datasets from 1920 to 2019. The dashed lines indicate $\pm 0.5\sigma$ thresholds of both indices, used to group the years into different subsamples.

similar in its design to the numerical experiments by Schubert et al. (2009), where the atmospheric general circulation models are forced with combinations of the AMV and PMV SST patterns. The seasonal AMV and PMV indices used here represent the mean indices averaged over four different SST datasets. Similarly, the seasonal precipitation and Tas anomalies also indicate the averaged response across the different datasets listed in Table 1.

TABLE 2. The years and mean PMV and AMV indices (the means of the PMV and AMV indices based on the HadSST3, ERSSTv5, Kaplan, and COBE datasets) for the composite cases considered in this study. The standard deviation is 0.160°C for the AMV index and 0.206°C for the PMV index.

Case name	Years	Mean PMV	Mean AMV
Pw	1925–40, 1979–97, 2018, 2019	0.236	−0.021
Pc	1920, 1921, 1946–60, 1966, 1969–76, 2003–13, 2015, 2016	−0.209	0.023
Aw	1929–50, 1953, 1956, 2000–19	−0.026	0.155
Ac	1920–23, 1966–94	0.076	−0.194
PwAw	1929–40, 2018, 2019	0.202	0.164
PwAc	1979–94	0.286	−0.181
PcAw	1946–50, 1953, 1956, 2003–13, 2015, 2016	−0.203	0.148
PcAc	1920, 1921, 1966, 1969–76	−0.192	−0.225

The combined impact of the PMV and AMV, for example the PwAw composite, contains the individual impacts from the Pw and Aw. These are considered as the zeroth-order processes. Because Pacific SST variability may influence Atlantic SST and vice versa (Cai et al. 2019), the composite for the PwAw case also contains the effect on South American climate from the footprint of the warm Pacific on the Atlantic SST, here referred to as Pw′Aw, and from Aw's footprint on the Pacific, referred to as PwAw′; these are considered as the first-order processes. Similarly, the composite for the PcAw case contains the effect from Pc's impact on the Atlantic (Pc′Aw) and from Aw's impact on the Pacific (PcAw′). To identify the PMV's impact on South America under a warm AMV, we calculate the difference of the composites between the PwAw and PcAw cases, which is

$$\begin{aligned}\mathrm{PwAw}-\mathrm{PcAw} &= (\mathrm{Pw}+\mathrm{Aw}+\mathrm{Pw}'\mathrm{Aw}+\mathrm{PwAw}')\\ &\quad-(\mathrm{Pc}+\mathrm{Aw}+\mathrm{Pc}'\mathrm{Aw}+\mathrm{PcAw}')\\ &= (\mathrm{Pw}-\mathrm{Pc})\times(1+\mathrm{Aw}')+(\mathrm{Pw}'-\mathrm{Pc}')\times\mathrm{Aw},\end{aligned} \tag{2}$$

where the first term on the right side represents the impact of the PMV (Pw − Pc) modulated by the Aw phase, and the second term on the right side represents the impact of the Aw modulated by the PMV phase difference (Pw′ − Pc′). To obtain the joint impact from PMV and a warm AMV (referred to as PMVAw), we will subtract (2) by the impacts of the PMV (Pw − Pc) under neutral AMV:

$$\begin{aligned}\mathrm{PMVAw} &= (\mathrm{PwAw}-\mathrm{PcAw})-(\mathrm{Pw}-\mathrm{Pc})\\ &= (\mathrm{Pw}-\mathrm{Pc})\times\mathrm{Aw}'+(\mathrm{Pw}'-\mathrm{Pc}')\times\mathrm{Aw}.\end{aligned} \tag{3}$$

This is done by comparing the (PwAw − PcAw) composite difference with the (Pw − Pc) composite difference (i.e., the PMV's impact under neutral AMV). Similarly, we can obtain the joint impacts for the other cases. For example, the joint impact from AMV and a warm PMV is quantified by comparing the (PwAw − PwAc) composite difference (i.e., the AMV's impact under a warm PMV) with the (Aw − Ac) composite difference (i.e., the AMV's impact under neutral PMV).

e. Statistical hypothesis testing

The statistical significance of the composite anomalies and correlation coefficients was assessed using a Monte Carlo permutation test with 10 000 random permutations (Nichols and Holmes 2002).

3. The individual and joint impacts of PMV and AMV on South American precipitation

a. JJA precipitation

To understand how the Atlantic and Pacific modes interact with one another and how they modulate each other's impact on South American climate, it is helpful to first briefly consider each mode in isolation by ignoring the conditions in the other basin. Table 2 shows that the indices of the other basin's mode are close to zero for our Pw, Pc, Aw and Ac individual cases that include all the years with a warm or cold condition in the corresponding basin, thus the influence from the other basin for these individual cases is likely small. This is verified by the similarity between our composite difference (i.e., Pw − Pc and Aw − Ac) and that using only the neutral years in the other basin (i.e., PwAn − PcAn and PnAw − PnAc; not shown).

For the Pw − Pc case (i.e., the impact from the PMV without a large influence from the AMV), large but noisy anomalies of JJA rainfall are seen over northern (north of 0°) South America and the southern Andes, with large wet anomalies around the Pacific coast between 28° and 40°S and around the Atlantic coast between 25° and 35°S (Fig. 2a); JJA precipitation is reduced over parts of the northern Amazon basin, though noisy, while slightly enhanced JJA precipitation extends from the southern Amazon basin to central and southern Brazil (Fig. 2a). These results generally agree with those presented in Garreaud et al. (2009), Dai (2013), Dong and Dai (2015), and Flantua et al. (2016).

To understand the joint impacts of the AMV and PMV on South American climate, we next look at the difference between one ocean forcing and two ocean forcing combinations. The differences between Figs. 2b and 2a and between Figs. 2c and 2a are indications of the joint impacts of the AMV and PMV on South American precipitation. In particular, when the AMV is in its cold phase, the precipitation response to the PMV is more negative over 0°–10°S and more positive over the northern Amazon basin (Fig. 2c) than the precipitation response to the PMV when the AMV's phase is ignored (Fig. 2a), while the precipitation response is weaker when the AMV is in its warm phase (Fig. 2b). This dipole pattern is seen in GPCC, UDelaware, and CRU TS datasets (Fig. 3). The dampened

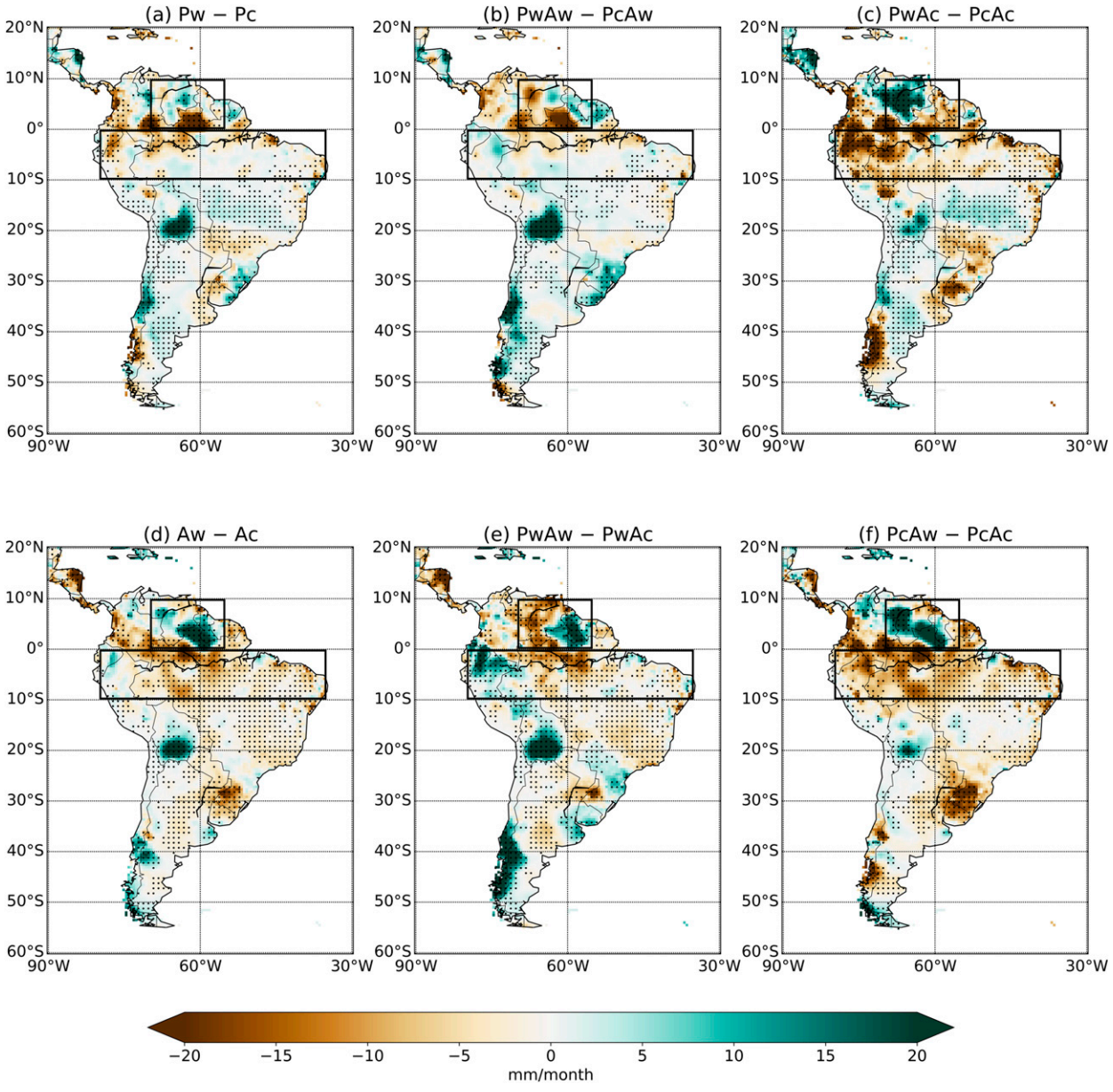

FIG. 2. The composite difference of (detrended and 11-yr moving averaged) JJA precipitation anomalies from 1920 to 2016 (relative to the 1920–2015 mean) between the (a) Pw and Pc, (b) PwAw and PcAw, (c) PwAc and PcAc, (d) Aw and Ac, (e) PwAw and PwAc, and (f) PcAw and PcAc. The precipitation anomalies represent the mean response averaged across the CRU TS, GPCC, and UDelaware datasets. The color shading shows the precipitation anomalies (mm month^{-1}). Stippling indicates regions where the precipitation difference is above the 99% confidence level. The rectangular boxes indicate the regions used to calculate the area-averaged precipitation anomalies in Fig. 3.

(strengthened) precipitation anomalies seen in Fig. 2b (Fig. 2c) between 0°and 10°S when compared to the Pw − Pc case (Fig. 2a) are associated with weaker (stronger) descending motion at these latitudes in the local Hadley circulation, shown in Fig. 4b (Fig. 4c). The weaker (stronger) descending motions are, in turn, related to the reduced (enhanced) ANSG shown in the PwAw − PcAw (PwAc − PcAc) SST composites (Figs. 5b,c) relative to the Pw − Pc composite (Fig. 5a). The weaker SST gradient is related to a reduced northward shift of the Atlantic ITCZ and hence anomalous ascending motion over 0°–10°S, while the stronger ANSG is associated with the opposite mechanism. A warm PMV tends to induce descending motion over the tropical Atlantic, and an Ac background can invigorate this perturbed Walker circulation, while an Aw tends to weaken this teleconnection (Meehl et al. 2021). Furthermore, in the zonal wind profiles,

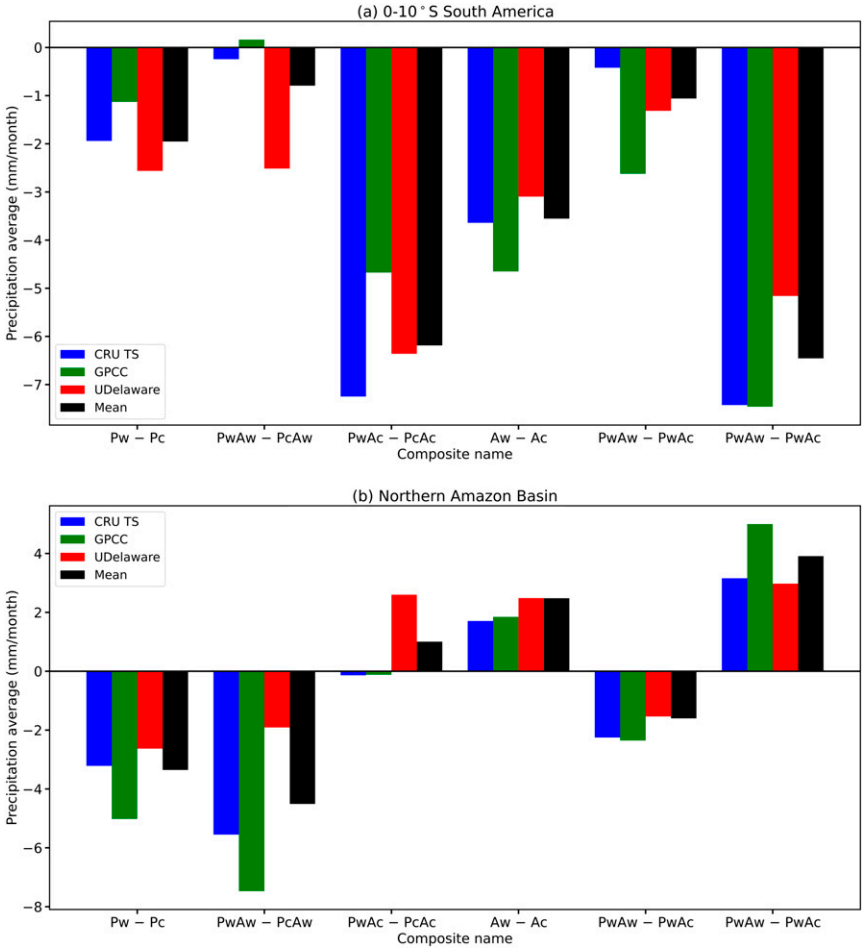

FIG. 3. Precipitation anomalies averaged over southern equatorial South America (0°–10°S, 35°–80°W) and the northern Amazon basin (0°–10°N, 55°–70°W) from the CRU TS, GPCC, UDelaware, and their means. The two regions are shown as black boxes in Fig. 2.

the local Walker circulation also shows anomalous ascending motion over northeastern Brazil (around 40°W) and the eastern equatorial Atlantic (east of 35°W) in the PwAw − PcAw case (Fig. 6b), while strong anomalous subsidence dominates over these regions in the PwAc − PcAc case (Fig. 6c). This is consistent with the more positive precipitation differences over northeastern Brazil in Fig. 2b than in Fig. 2c.

Next, we will focus on the results over subtropical South America. The precipitation response to the PMV during a cold AMV phase (PwAc − PcAc) is more positive over central Brazil, but more negative over southeastern South America (Fig. 2c) than the Pw − Pc case with neutral AMV (Fig. 2a), while the opposite is true when the AMV is in its warm phase (Fig. 2b). These changes appear to be part of a dipole pattern between the SACZ and rainfall over the subtropical plains in southeastern South America (Vera et al. 2006). The rainfall over the River Plate basin is associated with the intensity of the SALLJ. Negative outgoing longwave radiation (OLR) anomalies, which indicate enhanced convection, more cloud cover and hence more precipitation, extend from southeastern Brazil to the subtropical South Atlantic in the PwAc − PcAc composite (Fig. 5c), while these are less negative in the PwAw − PcAw composite (Fig. 5b). The negative OLR anomalies shown in Fig. 5c are associated with a strengthening of the SACZ, which promotes rainfall over central Brazil but suppresses rainfall over southeastern South America (Fig. 2c). The more positive OLR anomalies over central Brazil for the PwAw − PcAw composite (Fig. 5b) than the Pw − Pc composite (Fig. 5a) are consistent with the reduced rainfall over this region (Figs. 2a,b). The changes of the SACZ are related to the changes in the PSA pattern (not shown).

We next discuss how the PMV modulates the influence of the AMV on South American rainfall in JJA. The JJA precipitation composite for the Aw − Ac case shows generally negative values over much of South America south of the equator, except over northern Peru and the southern Andes, as well as positive values over parts of northern South America (Fig. 2d). The results are consistent with the results of Knight et al. (2006) and Flantua et al. (2016). When the PMV is in its

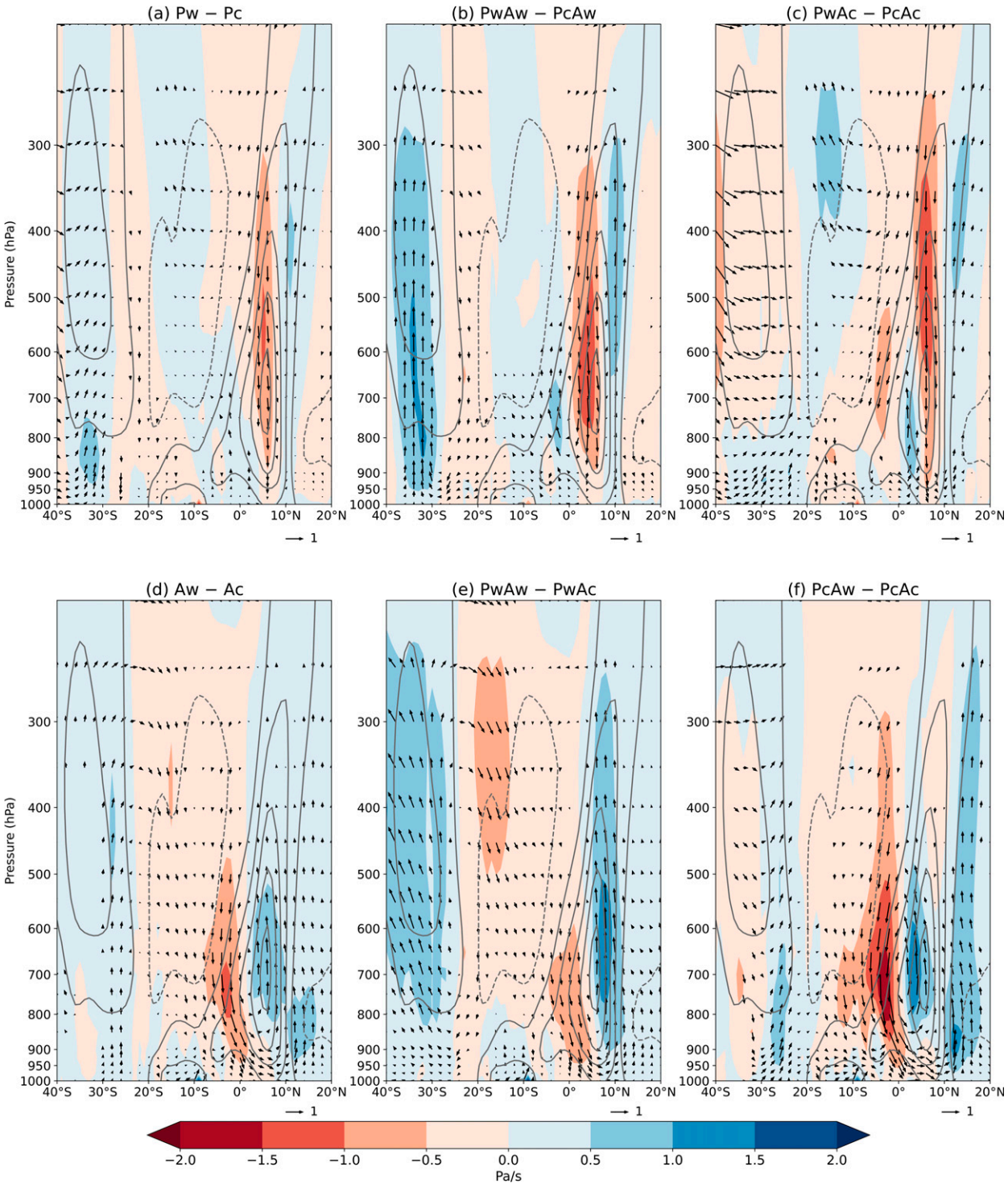

FIG. 4. The composite difference of anomalous (detrended and 11-yr moving averaged) JJA local Hadley circulation averaged over the 75°–35°W sector from 1920 to 2015 (relative to the 1920–2015 mean) from the 20CRv3 between the (a) Pw and Pc, (b) PwAw and PcAw, (c) PwAc and PcAc, (d) Aw and Ac, (e) PwAw and PwAc, and (f) PcAw and PcAc. A scaling factor of −200 was applied to the vertical pressure velocity (Pa s^{-1}) for visualization. The shading shows the magnitude of vertical velocity multiplied by −200 (in Pa s^{-1}, positive upward). Wind vectors are only shown where either meridional or vertical wind difference is above the 99% confidence level. The contours show the climatology of the vertical velocity with an interval of −600 Pa s^{-1}.

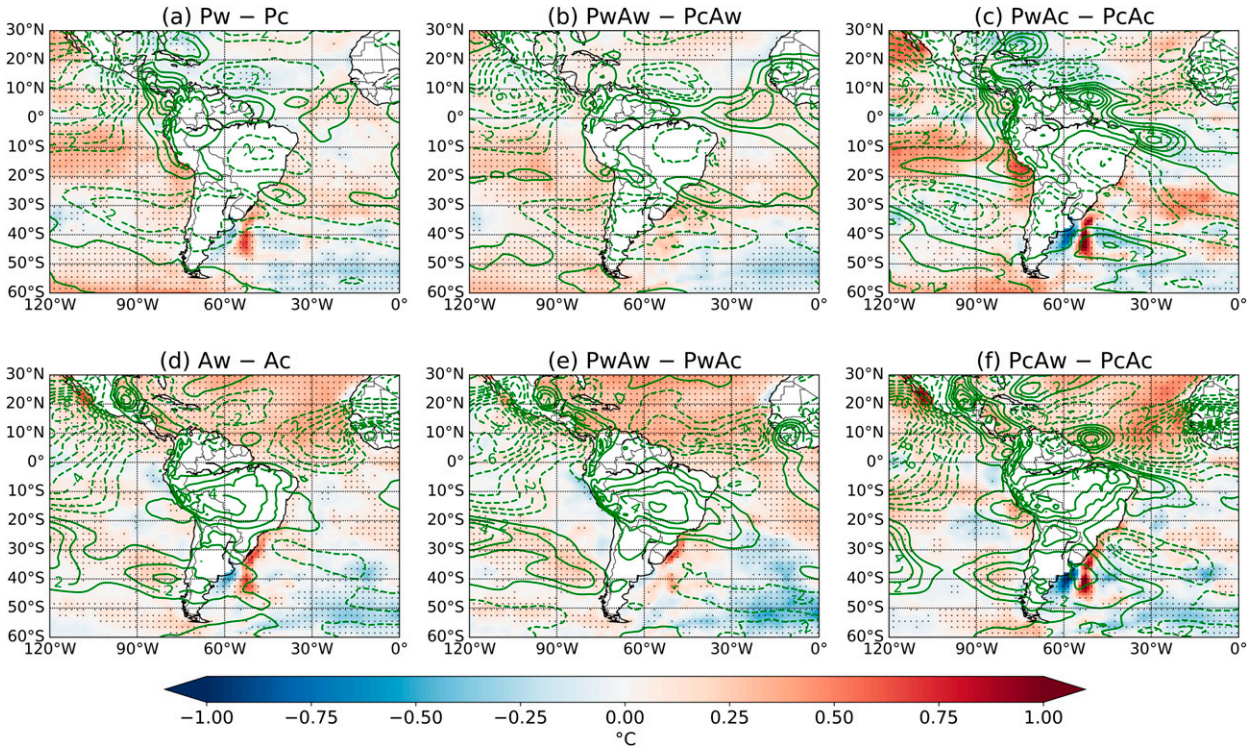

FIG. 5. The composite difference of (detrended and 11-yr moving averaged) JJA SST anomalies from 1920 to 2019 (relative to the 1920–2015 mean) from the HadISST, and the (detrended and 11-yr moving averaged) OLR anomalies from 1920 to 2015 (relative to the 1920–2015 mean) from the 20CR V3 between the (a) Pw and Pc, (b) PwAw and PcAw, (c) PwAc and PcAc, (d) Aw and Ac, (e) PwAw and PwAc, and (f) PcAw and PcAc. The color shading shows the SST anomalies (°C), and the contours show the OLR anomalies (W m^{-2}). The contour interval for OLR is 1 W m^{-2}; the zero contour for OLR is omitted. Stippling indicates the regions where the SST difference is above the 99% confidence level.

warm phase, the precipitation response to the AMV is less negative south of the equator, but drier over the northern Amazon basin than the Aw − Ac case with neutral PMV (Figs. 2d,e), while it is the opposite during the PMV cold phase (Fig. 2f). This dipole pattern is robust across the GPCC, UDelaware, and CRU TS datasets (Fig. 3). In the southern equatorial region (0°–10°S), the positive AMV impacts in the western part (Peru) are enhanced and the negative differences in the central-eastern part of the zone (Brazil) are reduced (Fig. 2e) when the PMV is in its warm phase, while the PcAw − PcAc difference (i.e., the joint impacts when the PMV is in its cold phase) shows the opposite response (Fig. 2f). The less (more) negative rainfall anomalies in the PwAw − PwAc (PcAw − PcAc) case are consistent with the weaker (stronger) descending motion over 0°–10°S seen in the local Hadley circulation (Figs. 4e,f) in response to a reduced (enhanced) ANSG. The SST composite for the PwAw − PwAc case (Fig. 5e) exhibits a weaker ANSG than the Aw–Ac composite (Fig. 5d), while the ANSG in the PcAw − PcAc composite (Fig. 5f) is enhanced. The warm phase of the PMV tends to warm the tropical Atlantic (Meehl et al. 2021), therefore the tropical South Atlantic SST difference is more positive in the PwAw − PwAc composite than in the PcAw − PcAc composite (Figs. 5e,f). Moreover, the local Walker circulation also exhibits an adjustment in response to PMV's phase: during the warm PMV phase, the subsidence over tropical South America is weaker over northeastern Brazil (around 40°W) and the western equatorial Atlantic (east of 35°W) compared with the Aw − Ac composite (Figs. 6d,e), while the descending motion is stronger during a cold PMV phase (Fig. 6f). In addition, when the PMV is in its warm phase, the AMV impact on rainfall over southeastern South America is more positive and the impact over central-eastern Brazil is more negative (Fig. 2e) than under neutral PMV conditions (Fig. 2d). In contrast, when the PMV is in its cold phase, the AMV impact on these regions is the opposite (Fig. 2f). These changes also appear to be part of the dipole pattern between the SACZ and southeastern South American rainfall. Indeed, there are large positive OLR anomalies extending from central Brazil to the subtropical South Atlantic in the PwAw − PwAc composite (Fig. 5e), while OLR anomalies over this region are less pronounced in the PcAw − PcAc composite (Fig. 5f) than the Aw − Ac composite (Fig. 5d), which is consistent with the observed changes in rainfall (Figs. 2d,f).

b. *DJF precipitation*

Here we analyze the precipitation response for the DJF season, which represents the main wet season over much of

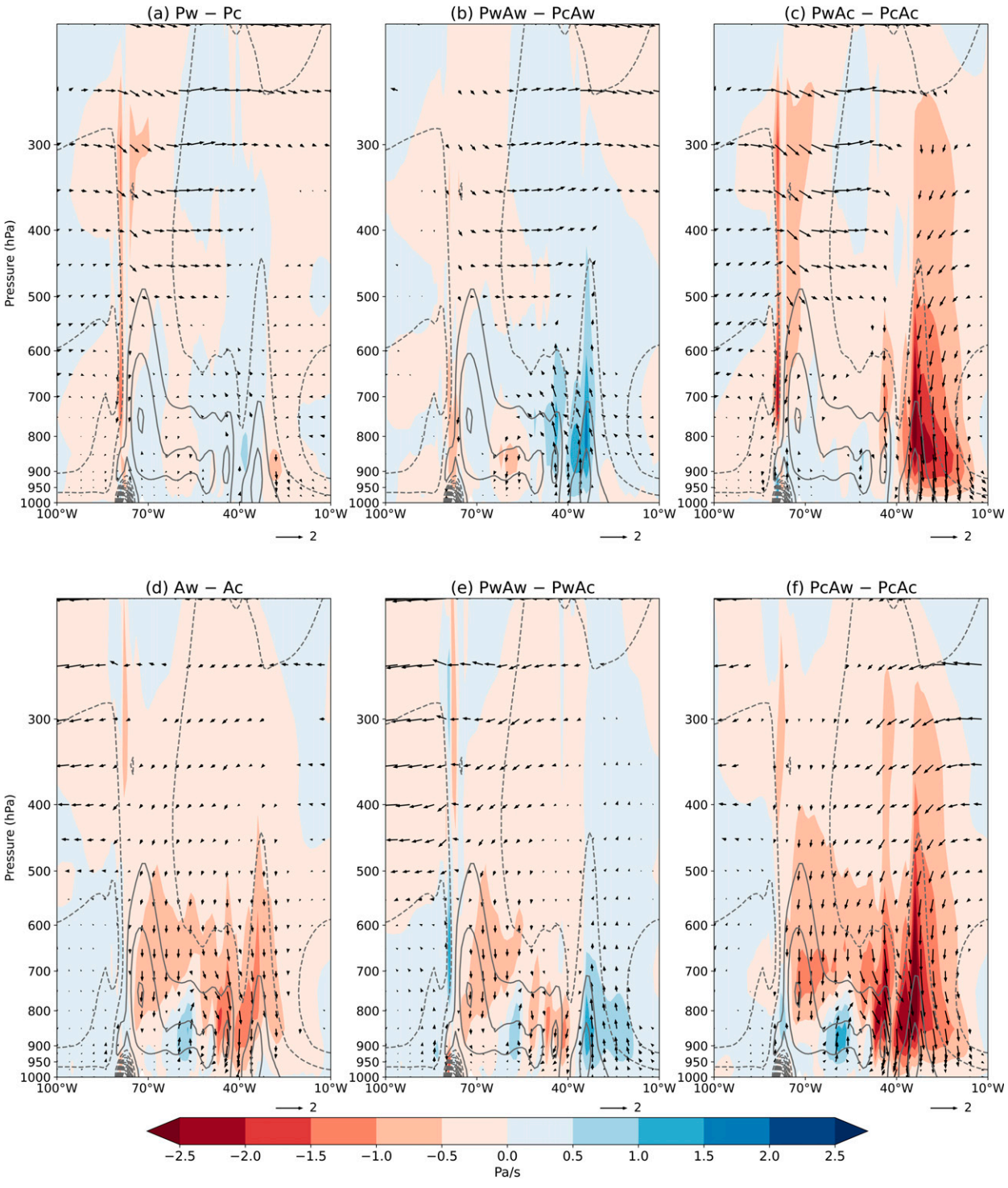

FIG. 6. The composite difference of anomalous (detrended and 11-yr moving averaged) JJA local Walker circulation averaged over the 10°S–0° sector from 1920 to 2015 (relative to the 1920–2015 mean) from the 20CRv3 between the (a) Pw and Pc, (b) PwAw and PcAw, (c) PwAc and PcAc, (d) Aw and Ac, (e) PwAw and PwAc, and (f) PcAw and PcAc. A scaling factor of −200 was applied to the vertical pressure velocity (Pa s^{-1}) for visualization. The shading shows the magnitude of vertical velocity multiplied by −200 (in Pa s^{-1}, positive upward). Wind vectors are only shown where either meridional or vertical wind difference is above the 99% confidence level. The contours show the climatology of the vertical velocity with interval of −600 Pa s^{-1}.

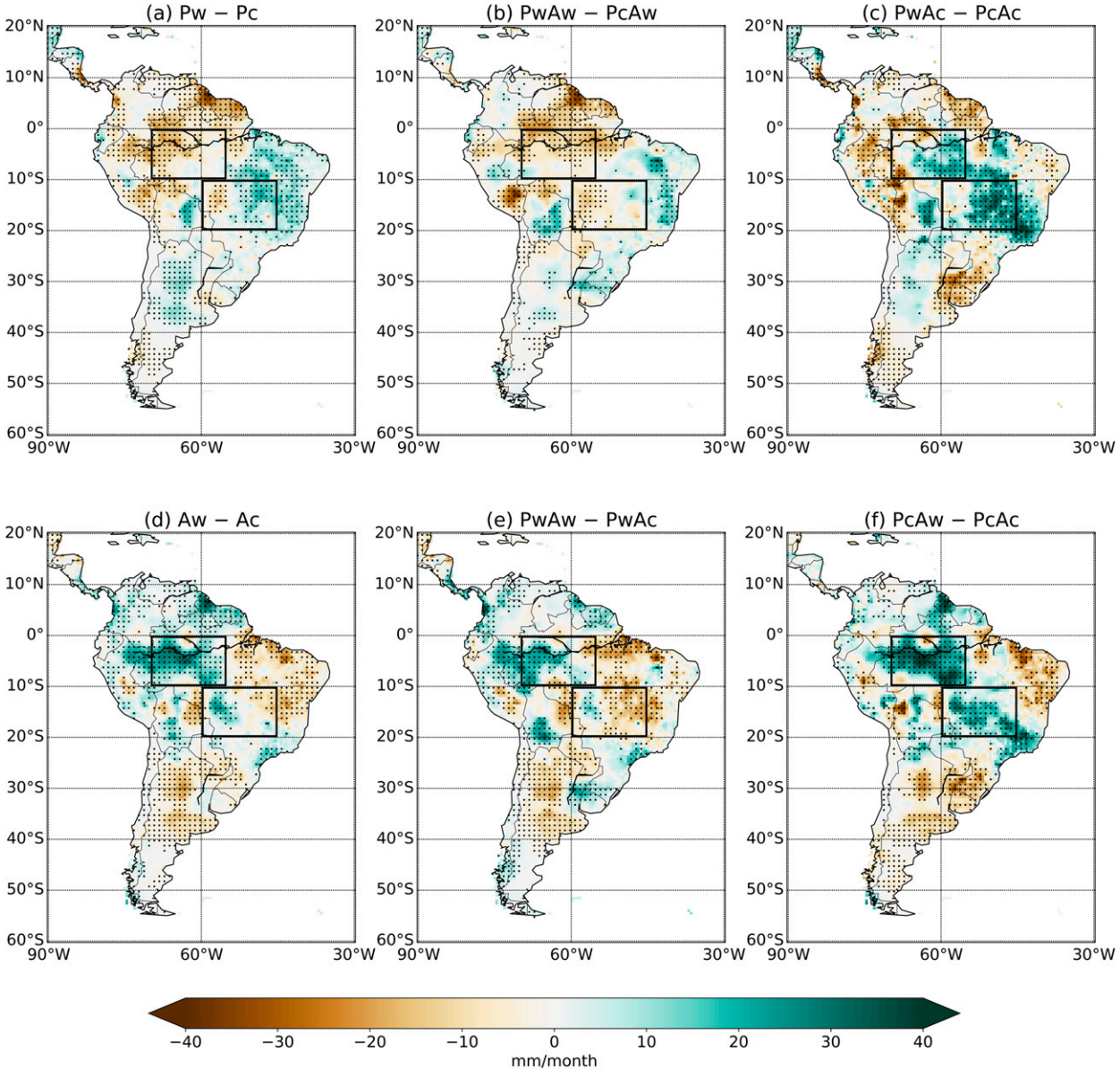

FIG. 7. The composite difference of (detrended and 11-yr moving averaged) DJF precipitation anomalies from 1920 to 2015 (relative to the 1920–2015 mean) between the (a) Pw and Pc, (b) PwAw and PcAw, (c) PwAc and PcAc, (d) Aw and Ac, (e) PwAw and PwAc, and (f) PcAw and PcAc. The precipitation anomalies represent the mean response averaged across the CRU TS, GPCC, and UDelaware datasets. The color shading shows the precipitation anomalies (mm month^{-1}). Stippling indicates the regions where the precipitation difference is above the 99% confidence level. The rectangular boxes indicate the regions used to calculate the area-averaged precipitation anomalies in Fig. 8.

tropical South America south of the equator, in conjunction with the mature phase of the SASM. The DJF rainfall response to the warm phase of the PMV is negative over northern South America north of the equator and over the Amazon basin, and positive over eastern and southern Brazil, eastern Bolivia, and northern Argentina (Fig. 7a). These results are generally consistent with those of Garreaud et al. (2009), Dai (2013), Dong and Dai (2015), Flantua et al. (2016), and Villamayor et al. (2018), except that our PMV index is positively correlated with precipitation over northeast Brazil, while their PMV indices show negative correlations over this region. The difference may be due to our focus on DJF precipitation here, while these other studies analyzed annual precipitation, thereby including the main wet season, which in this region is March–May.

We next examine the PwAw − PcAw and PwAc − PcAc composites, which represent the PMV-related precipitation patterns during the warm and cold phases of the AMV, respectively. The comparison of these patterns with the Pw − Pc

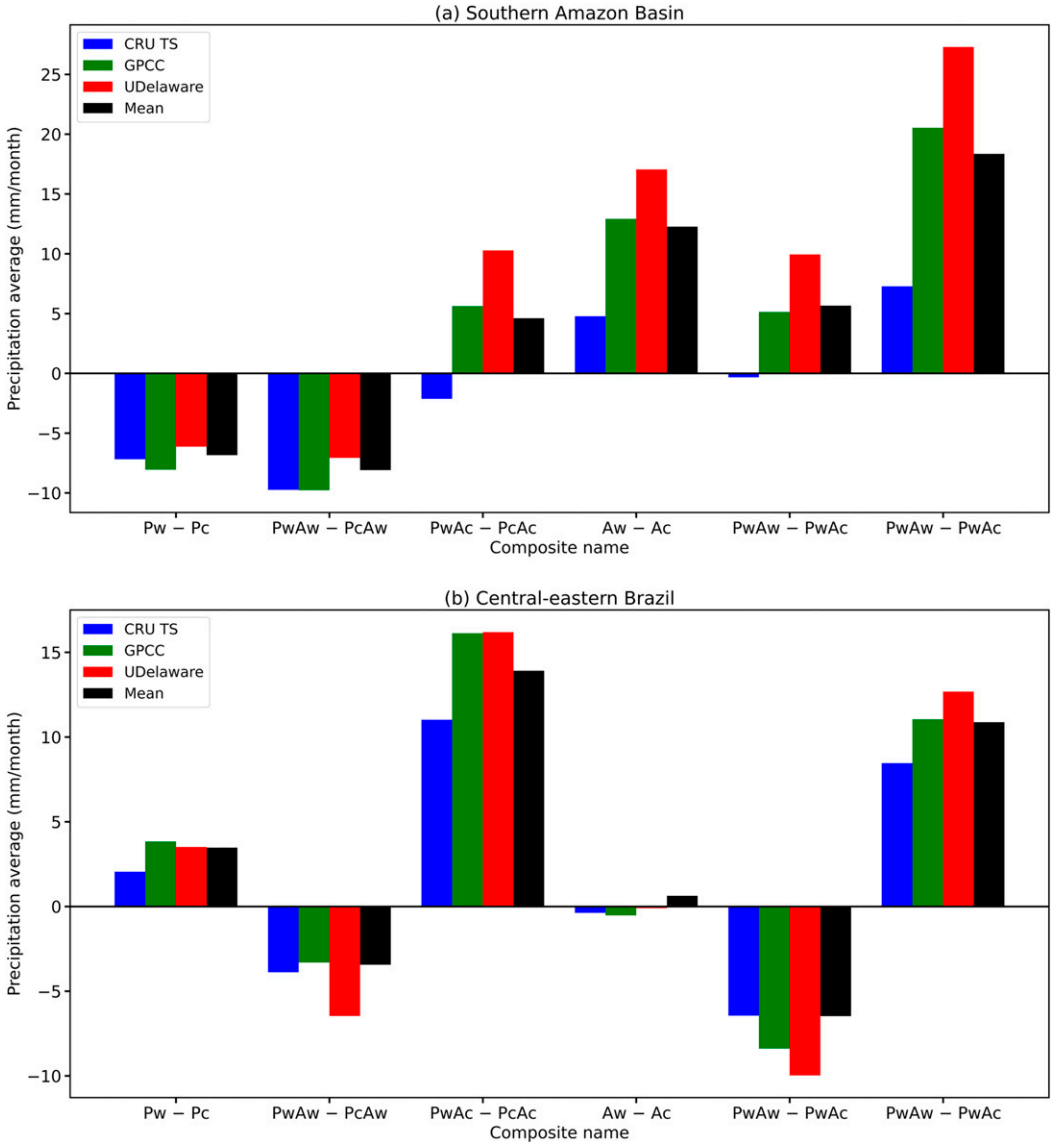

FIG. 8. Precipitation anomalies averaged over the southern Amazon basin (0°–10°S, 55°–70°W) and central-eastern Brazil (10°–20°S, 45°–60°W) from the CRU TS, GPCC, UDelaware, and their means. The two regions are shown as black boxes in Fig. 7.

composite reveals how the AMV modulates the PMV impact on South American precipitation in DJF. Figure 7b shows that the AMV in its warm phase enhances the PMV influence on DJF precipitation, with anomalous drying over the central Amazon basin and central-eastern Brazil and wetting over northeast Brazil and southeastern South America. In contrast, during the cold phase of the AMV, the PMV influence over the central Amazon basin and central-eastern Brazil is more positive, while the differences over northeastern Brazil and southeastern South America are more negative (Fig. 7c). The rainfall changes observed over the Amazon basin and central-eastern Brazil are robust across the GPCC, UDelaware, and CRU TS datasets (Fig. 8). The more negative (positive) PMV-related DJF rainfall anomalies over central-eastern Brazil during the warm (cold) AMV phase are associated with the reduced (enhanced) PMV-related anomalous ascending motion over eastern (60°–35°W) South America between 10° and 20°S in the local Hadley circulation (Figs. 9a–c). The local Walker circulation also shows stronger (weaker) subsidence around 50°W (60°W) during a warm (cold) AMV (Figs. 10b,c) than under neutral AMV conditions (Fig. 10a), which contributes to more negative (positive) precipitation anomalies over the eastern (central) Amazon basin (Figs. 7b,c). The anomalous local Hadley and Walker circulations are similar in the ERA5 data (not shown). Furthermore, the spatial pattern of the precipitation anomalies in Figs. 7b and 7c, which extends

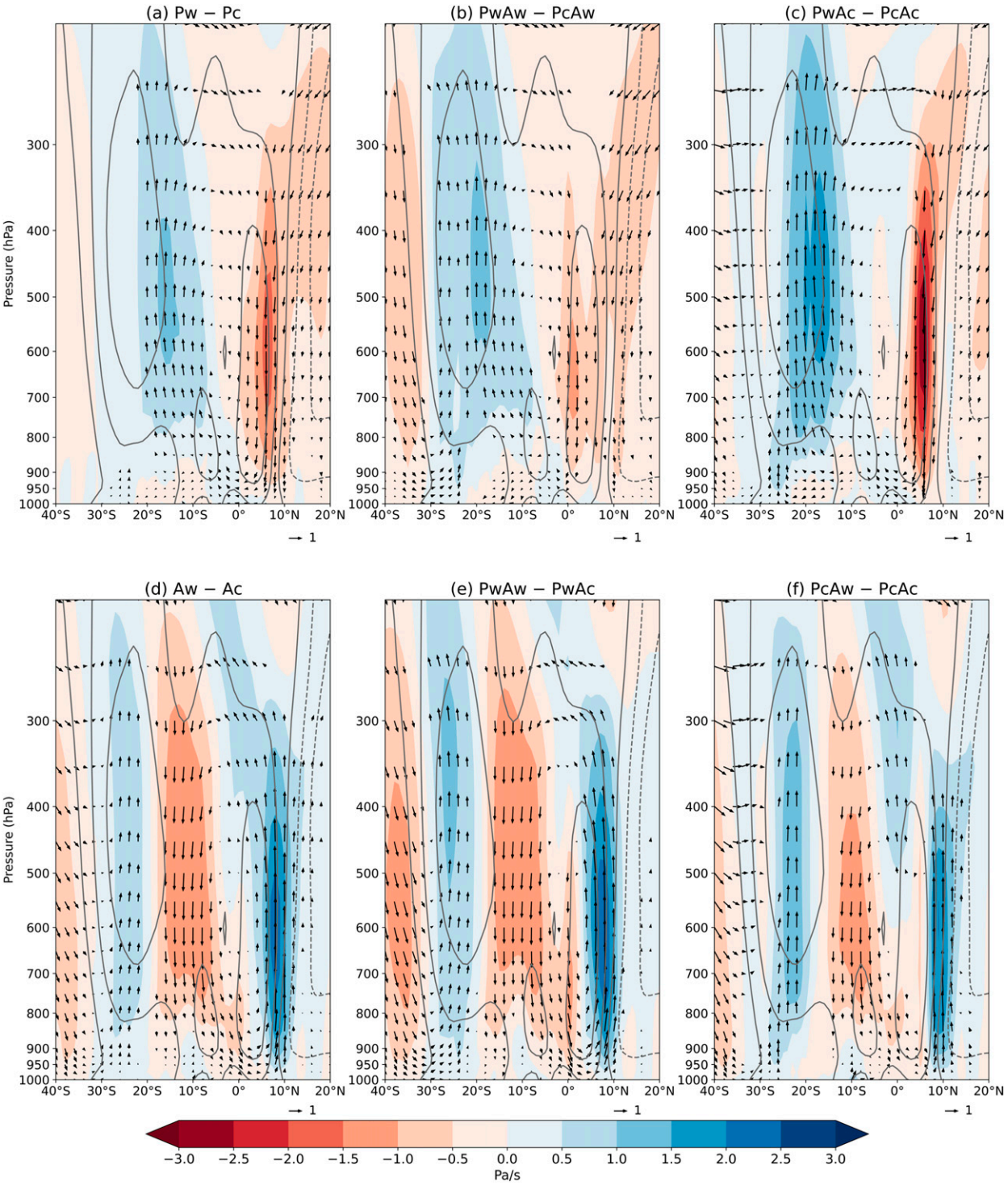

FIG. 9. The composite difference of anomalous (detrended and 11-yr moving averaged) DJF local Hadley circulation averaged over the 60°–35°W sector from 1920 to 2014 (relative to the 1920–2014 mean) from the 20CRv3 between the (a) Pw and Pc, (b) PwAw and PcAw, (c) PwAc and PcAc, (d) Aw and Ac, (e) PwAw and PwAc, and (f) PcAw and PcAc. A scaling factor of −200 was applied to the vertical pressure velocity (Pa s^{-1}) for visualization. The shading shows the magnitude of vertical velocity multiplied by −200 (in Pa s^{-1}, positive upward). Wind vectors are only shown where either meridional or vertical wind difference is above the 99% confidence level. The contours show the climatology of the vertical velocity with interval of −600 Pa s^{-1}.

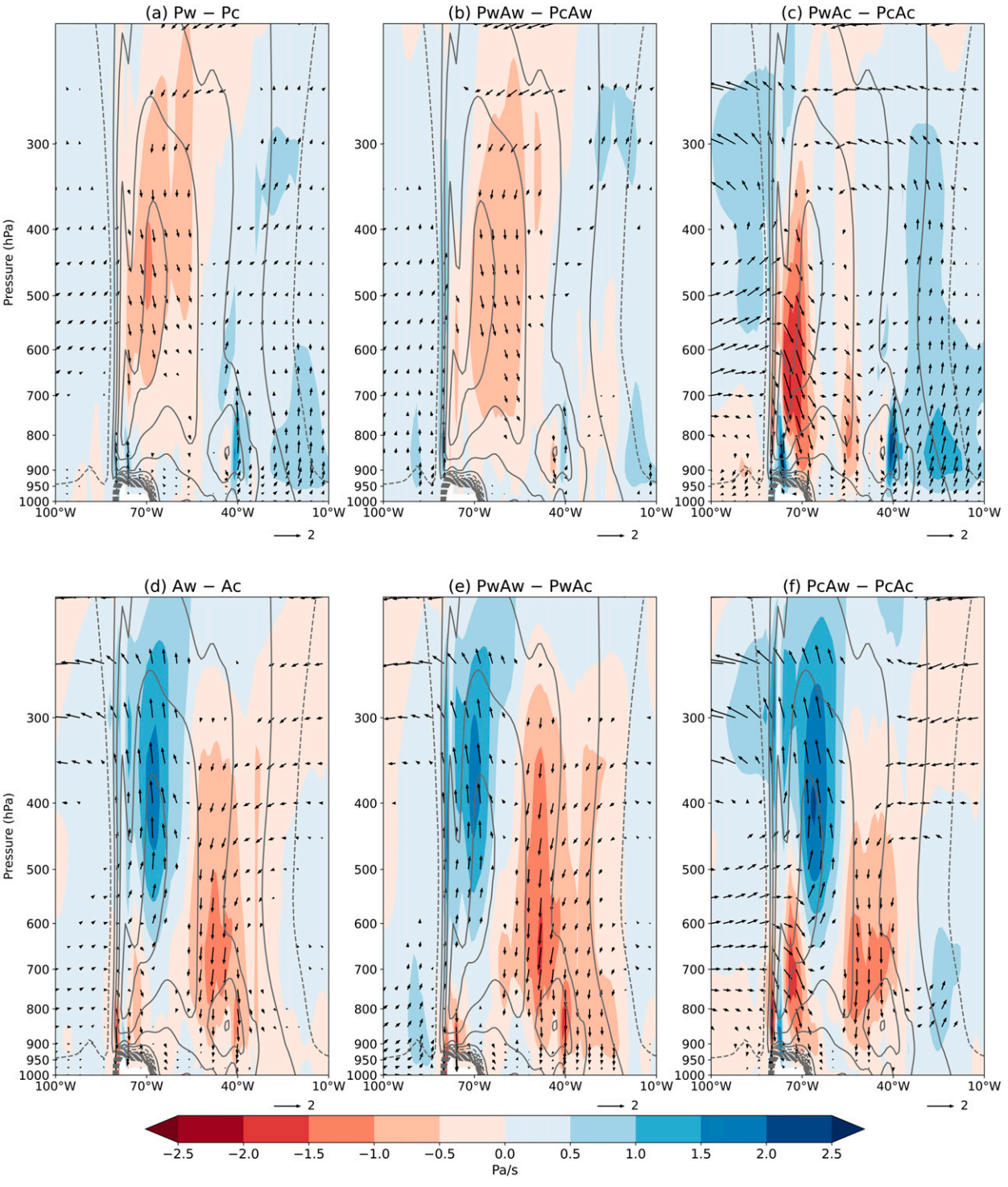

FIG. 10. The composite difference of anomalous (detrended and 11-yr moving averaged) DJF local Walker circulation averaged over the 10°S–0° sector from 1920 to 2014 (relative to the 1920–2014 mean) from the 20CRv3 between the (a) Pw and Pc, (b) PwAw and PcAw, (c) PwAc and PcAc, (d) Aw and Ac, (e) PwAw and PwAc, and (f) PcAw and PcAc. A scaling factor of −200 was applied to the vertical pressure velocity (Pa s^{-1}) for visualization. The shading shows the magnitude of vertical velocity multiplied by −200 (in Pa s^{-1}, positive upward). Wind vectors are only shown where either meridional or vertical wind difference is above the 99% confidence level. The contours show the climatology of the vertical velocity with interval of −600 Pa s^{-1}.

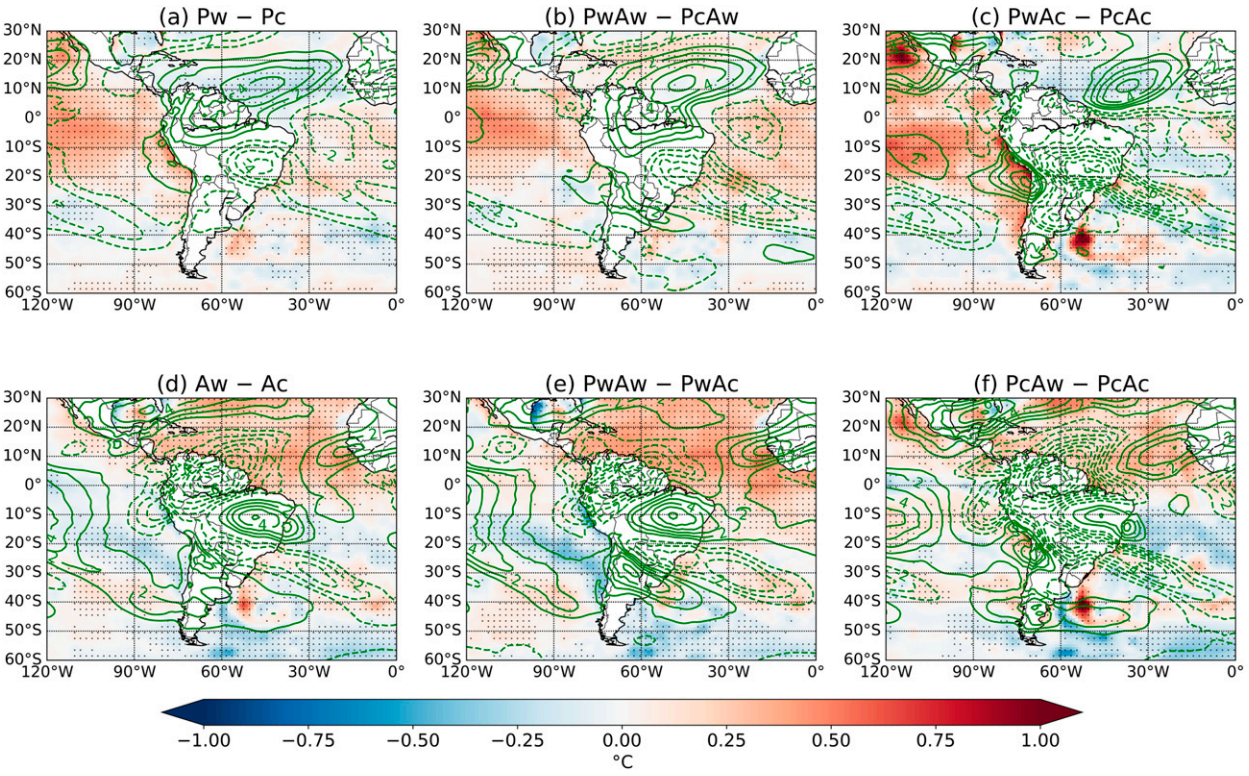

FIG. 11. The composite difference of (detrended and 11-yr moving averaged) DJF SST anomalies from 1920 to 2019 (relative to the 1920–2015 mean) from the HadISST, and the (detrended and 11-yr moving averaged) OLR anomalies from 1920 to 2014 (relative to the1920–2014 mean) from the 20CR V3 between the (a) Pw and Pc, (b) PwAw and PcAw, (c) PwAc and PcAc, (d) Aw and Ac, (e) PwAw and PwAc, and (f) PcAw and PcAc. The color shading shows the SST anomalies (°C), and the contours show the OLR anomalies (W m^{-2}). The contour interval for OLR is 1 W m^{-2}; the zero contour for OLR is omitted. Stippling indicates regions where the SST difference is above the 99% confidence level.

from the Amazon basin toward central-eastern Brazil in both cases, is reminiscent of the weakening and intensification of the SACZ. Indeed, strong negative OLR anomalies dominate in the PwAc − PcAc case (Fig. 11c) over the SACZ region, with the anomalies extending from the southern Amazon basin to the subtropical South Atlantic, consistent with the more positive rainfall anomalies over this region in the PwAc − PcAc composite (Fig. 7c). On the other hand, the OLR anomalies indicate a weakened and southward displaced SACZ in the PwAw − PcAw composite (Fig. 11b), resulting in drier conditions over central-eastern Brazil, but wetter conditions further south, between 25° and 35°S (Fig. 7b). These SACZ changes are associated with changes in the PSA pattern (not shown).

Figure 7d shows that the AMV's impact on DJF rainfall is approximately the opposite of the PMV's impact (Fig. 7a) over many regions, such as the Amazon basin, northeastern Brazil, southern Brazil, and northern Argentina. This pattern is generally consistent with the results of Knight et al. (2006), Flantua et al. (2016), and Villamayor et al. (2018) for tropical South America, except that our result shows positive values over the central Amazon basin, while theirs show negative values over this region. The difference may result from our focus on the DJF season, while the other studies analyzed data from March–April–May, annual data, and from December to May, respectively. The roughly opposite anomaly patterns of DJF rainfall induced by the PMV and AMV likely result from teleconnections between the Pacific and Atlantic Ocean, such as La Niña-like SST patterns in the Pacific induced by a warm tropical North Atlantic (Li et al. 2016; Ruprich-Robert et al. 2017; Cai et al. 2019). Indeed, the Aw (Ac) phase tends to coincide with the Pc (Pw) phase (Fig. 1c and Table 2).

Differences between Figs. 7e and 7f reveal that the AMV influence on DJF rainfall over South America is strongly conditioned on the concurrent PMV phase. When the PMV is in its warm phase the AMV-related rainfall anomalies stretching from the Amazon basin to central-eastern Brazil are more negative, and the anomalies over northeastern and southeastern South America are more positive (Figs. 7d,e). In contrast, when the PMV is in its cold phase, the opposite precipitation changes occur over these regions, except the eastern Amazon basin (Figs. 7d,f), largely amplifying the AMV impacts shown in Fig. 7d. The more negative rainfall anomalies over central-eastern Brazil in the PwAw − PwAc composite and the more positive anomalies in the PcAw − PcAc composite can be attributed to, respectively, the stronger and weaker descending motion over eastern (60°–35°W) South America between 10° and 20°S in the local Hadley circulation

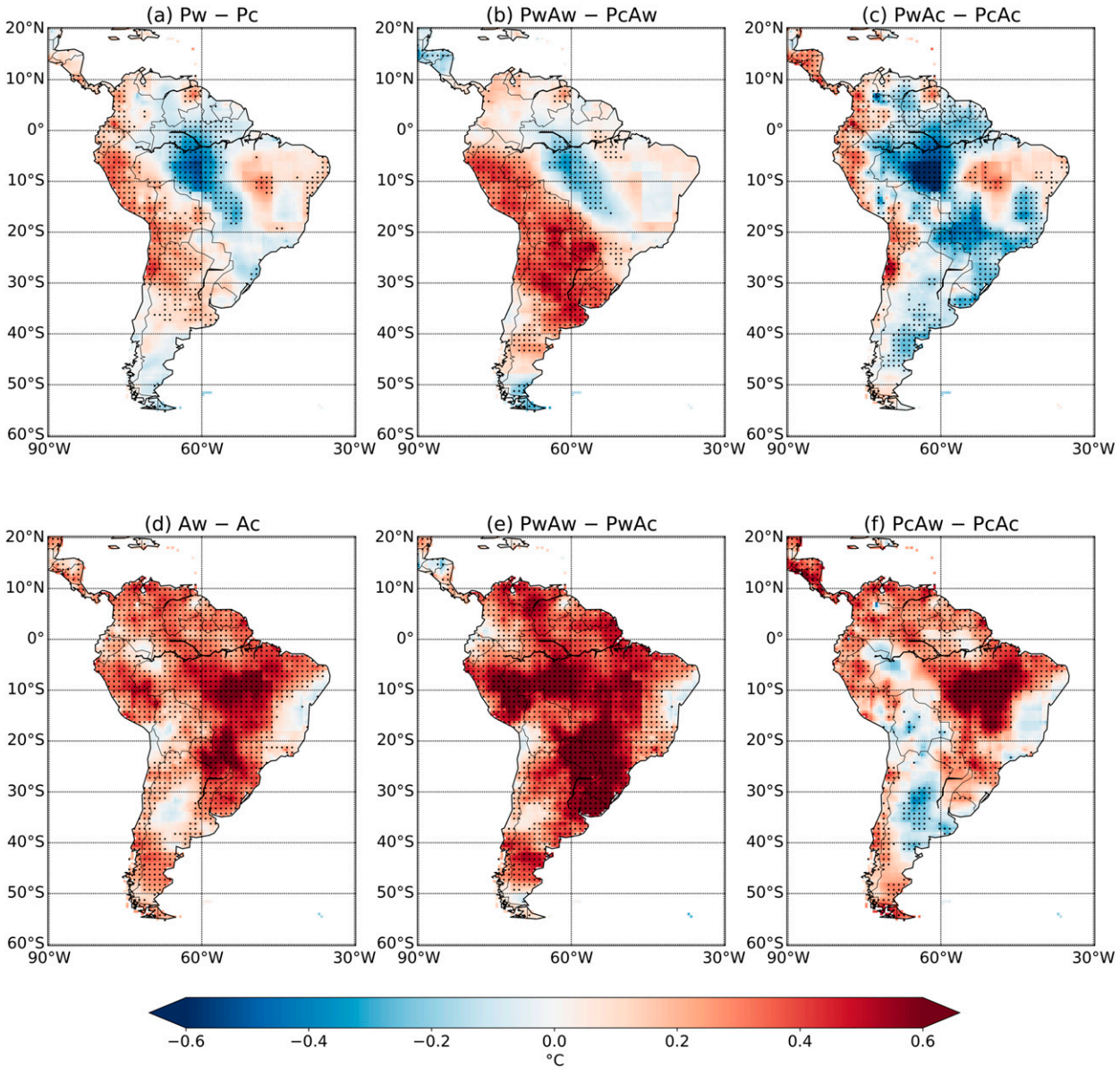

FIG. 12. The composite difference of (detrended and 11-yr moving averaged) JJA temperature anomalies from 1920 to 2017 (relative to the 1920–2015 mean) between the (a) Pw and Pc, (b) PwAw and PcAw, (c) PwAc and PcAc, (d) Aw and Ac, (e) PwAw and PwAc, and (f) PcAw and PcAc. The temperature anomalies represent the mean response averaged across the CRU TS, GISTEMP, and UDelaware datasets. The color shading shows the temperature anomalies (°C). Stippling indicates the regions where the temperature difference is above the 99% confidence level.

(Figs. 9d–f). This difference is also reflected in the stronger positive OLR anomalies centered over central-eastern Brazil in the PwAw − PwAc case (Fig. 11e) than the Aw − Ac case (Fig. 11d), and especially when compared to the PcAw − PcAc case (Fig. 11f). The anomalous OLR dipole pattern over eastern Brazil indicates a southward shift of the SACZ. The more negative (positive) precipitation anomalies over the Amazon basin under a warm (cold) PMV (Figs. 7e–f) can be attributed to differences in the local Walker circulation. Compared with the Aw − Ac case (Fig. 10d), convection around 65°W weakens in the PwAw − PwAc case (Fig. 10e) but strengthens in the PcAw − PcAc case (Fig. 10f). The relative changes in the local Hadley and Walker circulation anomalies based on the ERA5 dataset are similar (not shown).

4. The impacts on South American temperature

Finally, we also briefly examine the joint impacts of the AMV and PMV on South American Tas for the JJA and DJF seasons. Compared with a cold phase of the PMV, a warm

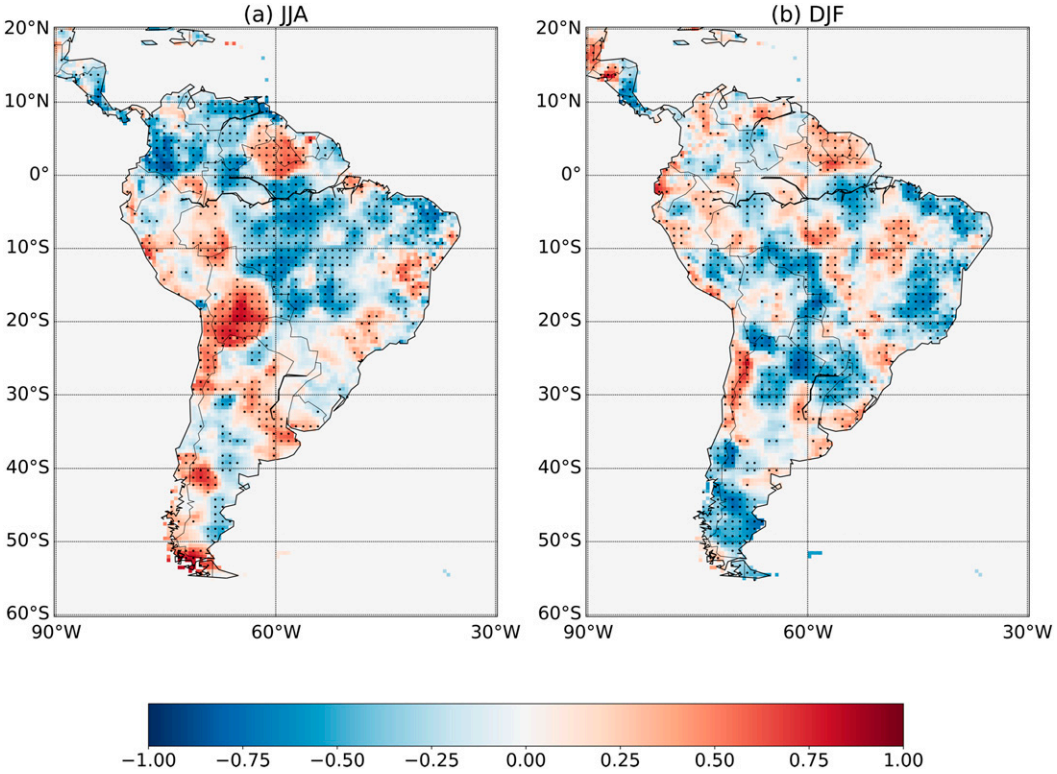

FIG. 13. Correlation maps between (detrended and 11-yr moving averaged) temperature anomalies (relative to the 1920–2015 mean) and precipitation anomalies (relative to the1920–2015 mean) during (a) JJA and (b) DJF from 1920 to 2016. Temperature anomalies are based on the mean across all temperature datasets (CRU TS, GISTEMP, and UDelaware) and precipitation anomalies are based on the mean across all rainfall datasets (CRU TS, GPCC, and UDelaware). The color shading shows the correlation coefficient. Stippling indicates the regions where the correlation coefficient is above the 99% confidence level.

PMV phase tends to reduce JJA Tas over the central Amazon basin, with the cooling extending toward southeastern Brazil, while positive Tas anomalies dominate along the Pacific coast, the tropical and subtropical Andes, northeastern Brazil, and northern and central Argentina (Fig. 12a). In contrast, a warm AMV phase induces positive JJA Tas anomalies over most of South America, with the largest warming covering most of Brazil, Peru, and Paraguay (Fig. 12d). The Tas anomaly patterns shown in Fig. 12a are broadly consistent with the PMV and annual Tas correlation patterns shown by Dong and Dai (2015, 2017). Garreaud et al. (2009) and Flantua et al. (2016) showed that the unsmoothed PMV indices are positively correlated with annual Tas over northern South America, the western coast of South America, and the Andes. Their results are for the most part consistent with ours, except for the central Amazon basin. Most likely the inconsistency occurs because here we focus on decadal-scale variability stratified by season, while the two prior studies focused on the interannual signals averaged over a full year (thus their results are not representative of the PMV-induced variations). Flantua et al. (2016) showed that the AMV index is positively correlated with annual Tas over South America north of 10°S, the northern Andes, and Paraguay, which mostly agrees with our Fig. 12d.

We next focus on the joint impacts of the AMV and PMV on South American temperature in JJA. Comparing Figs. 12b and 12c with Fig. 12a, we can see that their patterns are broadly similar, but the PMV impacts over South America are more positive under a warm AMV phase (Fig. 12b) and more negative under a cold AMV phase (Fig. 12c) than when the AMV phase is neutral (Fig. 12a). Similarly, a warm PMV phase makes the Tas response to the AMV more positive (Fig. 12e) and a negative PMV phase results in a more negative or less positive Tas response (Fig. 12f). Furthermore, it is worth noting that there appear to be some regions where the temperature response may be related to the precipitation changes. For example, the enhanced negative temperature anomalies over the SACZ region of central-eastern Brazil between 10° and 20°S in the PwAc − PcAc case (Figs. 12a,c) correspond to the regions with more positive precipitation for the same case (Figs. 2a,c). Indeed, the JJA precipitation and temperature anomalies show significant negative correlations over this region (Fig. 13a), suggesting that the surface cooling may result from increased cloud cover and/or increased surface evaporation due to increased soil moisture induced by the increased rainfall (Barros et al. 2002; Trenberth and Shea 2005).

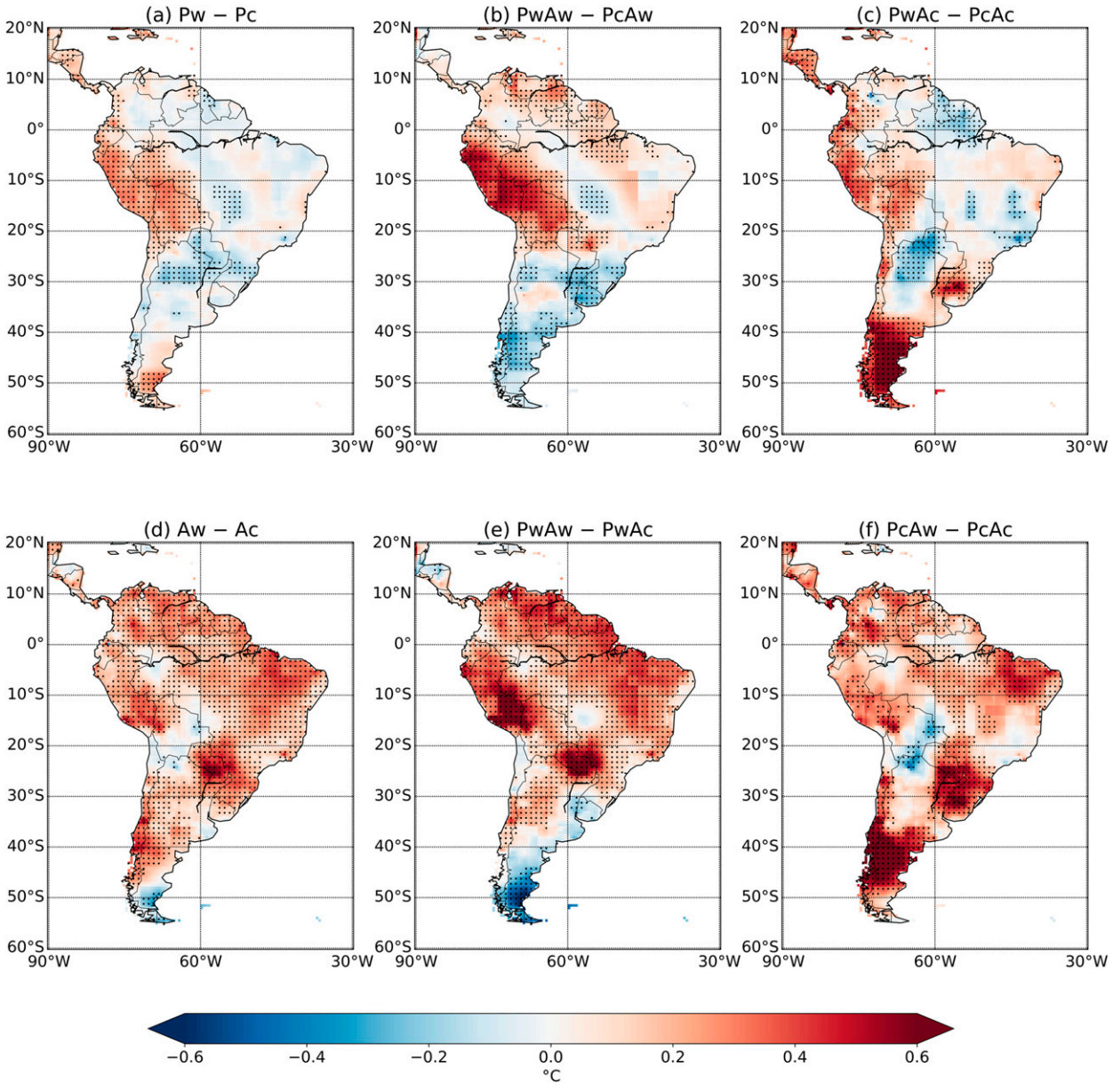

FIG. 14. As in Fig. 12, but for (detrended and 11-yr moving averaged) DJF temperature anomalies from 1920 to 2016 (relative to the1920–2015 mean). The temperature anomalies represent the mean response averaged across the CRU TS, GISTEMP, and UDelaware datasets.

The PMV tends to increase (reduce) DJF Tas over western (southeastern) South America, which differs from the PMV impacts on JJA Tas (Figs. 12a and 14a). The AMV impacts on DJF Tas (Fig. 14d) broadly resemble the AMV impacts on JJA Tas (Fig. 12d) except over northern Argentina, eastern Brazil, and southernmost South America. Figures 14a and 14b show that during the warm AMV phase, the Tas anomalies associated with the PMV over South America north of 20°S are more positive. In turn, during the cold AMV phase the warming over Bolivia is weakened, and the Tas increase associated with the PMV across southern South America intensifies and expands (Fig. 14c). Along the Atlantic coast of Brazil and in Patagonia, the temperature anomalies associated with the PMV reverse sign, depending on the phase of the AMV (Figs. 14b,c). PMV's phase also has noticeable effects on AMV's impact on DJF Tas over parts of South America. For example, when the PMV is in its warm phase the AMV's warming effect over South America north of 20°S is strengthened, but there is a stronger cooling effect over the southern tip of South America (Fig. 14e), whereas a cold PMV mainly enhances AMV's cooling effect over Bolivia and warming effect over southeastern and southern South America (Fig. 14f). A negative correlation

between temperature and precipitation occurs over southeastern and southernmost South America (Fig. 13b), which is consistent with the colder and wetter conditions resulting from both the PMV's impacts under a warm AMV (Figs. 14b and 7b) and the AMV's impact under a warm PMV phase (Figs. 14e and 7e), as well as the warmer and drier conditions resulting from both the PMV's impact under a cold AMV (Figs. 14c and 7c) and AMV's impact under a cold PMV phase (Figs. 14f and 7f).

5. Summary and discussion

Observational and reanalysis data were analyzed to examine the impacts of warm and cold phases of the PMV and AMV and their various combinations on precipitation and Tas over South America during DJF and JJA. Our focus was on documenting how PMV-induced anomaly patterns were modulated by the phase of the AMV and how the AMV-induced changes were modulated by the phase of the PMV, rather than the physical processes through which the AMV and PMV interact with each other and thus lead to different impacts over South America under their different phase combinations. Idealized numerical experiments with prescribed SST fields in one ocean basin while allowing coupled interactions in the other, may be better suited for such an investigation (Li et al. 2016; Ruprich-Robert et al. 2017; Meehl et al. 2021).

Nonetheless, our composite analyses suggest that the PMV- and AMV-related precipitation anomaly patterns over South America can be modulated by the concurring multidecadal SST phase in the other basin through changes in the ANSG, changes in the local Hadley and Walker circulation over tropical South America, as well as changes in intensity and location of the SACZ.

The temperature anomalies over South America resulting from the joint impacts of the PMV and AMV are also documented. In JJA, the temperature over central Brazil is negatively correlated with local precipitation; while in DJF, the temperature and precipitation over southern Bolivia and northern Argentina also share such a relationship. The cooling effect of cloud cover and increased soil moisture, enhancing surface evaporative cooling, which all increase with rainfall, may be causing the anticorrelation seen between temperature and precipitation.

Our composite results show that during JJA, the impact on AMV- or PMV-induced precipitation anomalies by the mode in the other basin shows similar dipole patterns that exhibit opposite anomalies between the northern Amazon basin and 0°–10°S, and between central Brazil and southeastern South America. Specifically, during a warm (cold) AMV phase the PMV-induced precipitation anomalies are more positive (negative) over the latitude band 0°–10°S but more negative (positive) over the northern Amazon, and they are more positive (negative) over southeastern South America but negative (positive) over central Brazil. PMV's impact on AMV-induced precipitation anomalies shows similar dipole patterns, despite the different precipitation anomaly patterns induced by AMV and PMV when the other basin is in a neutral phase. The first dipole pattern is related to the changes in the ANSG and the meridional displacement of the Atlantic ITCZ and the local Hadley circulation. The second dipole is associated with the intensity of the SACZ. Moreover, the PMV- and AMV-induced JJA temperature anomalies are more positive (negative) over entire South America when the other basin's mode is in its warm (cold) phase.

During DJF, the PMV's or AMV's modulation of the influence from the other basin also shows two dipole patterns that reveal opposite precipitation anomalies between the central Amazon basin and northeast Brazil, and between central-eastern Brazil and southeastern South America. Specifically, during a warm (cold) AMV phase the PMV-induced DJF precipitation anomalies are more negative (positive) over the central Amazon basin and central-eastern Brazil but more positive (negative) over northeast Brazil and southeastern South America. PMV's impact on AMV-induced DJF precipitation anomalies show similar dipole patterns. The changes of Amazonian rainfall are related to perturbations of the local Walker circulation over South America. The second dipole is associated with the meridional shift of the local Hadley circulation and changes in SACZ intensity. Furthermore, the PMV- and AMV-induced DJF temperature anomalies are more positive (negative) over the central Andes and central-eastern Brazil but more negative (positive) over southeastern South America and Patagonia when the other basin mode is in its warm (cold) phase.

Our PMV- and AMV-related precipitation and temperature composites are generally consistent with previous studies (Knight et al. 2006; Garreaud et al. 2009; Dai 2013; Dong and Dai 2015, 2017; Flantua et al. 2016; Villamayor et al. 2018). Some differences in the results of precipitation and temperature anomalies between our analysis and earlier studies may result from our focus on seasonal time scales while prior studies used annual means, or because here we emphasized the low-frequency component of AMV and PMV variability, while in previous research the interannual variability was not explicitly removed from these modes.

When considered in isolation, as was commonly done in previous studies, the precipitation and temperature fingerprints of the PMV and AMV over South America document a mean anomaly response, but our analysis indicates that significant departures from this fingerprint occur, depending on the phase state of the other ocean basin. We also emphasize the need to use low-frequency, smoothed indices of the PMV and AMV to extract the multidecadal temperature and precipitation fingerprints of these modes over South America. If the high-frequency interannual component is not removed, the composite fields will be dominated by the interannual signal instead and the results may look quite different. In essence, our results highlight the need to consider the influence of Pacific and Atlantic multidecadal variability in a joint framework.

Acknowledgments. This study was supported by NSF-PIRE (OISE-1743738) and NSF-P2C2 (AGS-1702439). A. Dai was also supported by the NSF Grant AGS-2015780 and the U.S. National Oceanic and Atmospheric Administration (Grant NA18OAR4310425). The authors deeply appreciate CIRES, CRU, GPCC, IRI, JMA, NASA GISS, NOAA, University of

Delaware, and the Met Office Hadley Center for providing the data.

Data availability statement. All data used in this study are available from public domain sites. Links to accessing all the datasets are provided in Table 1.

REFERENCES

Agudelo, J., P. A. Arias, S. C. Vieira, and J. A. Martínez, 2019: Influence of longer dry seasons in the Southern Amazon on patterns of water vapor transport over northern South America and the Caribbean. *Climate Dyn.*, **52**, 2647–2665, https://doi.org/10.1007/s00382-018-4285-1.

Arias, P. A., R. Fu, C. Vera, and M. Rojas, 2015: A correlated shortening of the North and South American monsoon seasons in the past few decades. *Climate Dyn.*, **45**, 3183–3203, https://doi.org/10.1007/s00382-015-2533-1.

Barichivich, J., E. Gloor, P. Peylin, R. J. W. Brienen, J. Schöngart, J. C. Espinoza, and K. C. Pattnayak, 2018: Recent intensification of Amazon flooding extremes driven by strengthened Walker circulation. *Sci. Adv.*, **4**, eaat8785, https://doi.org/10.1126/sciadv.aat8785.

Barros, V. R., A. M. Grimm, and M. E. Doyle, 2002: Relationship between temperature and circulation in southeastern South America and its influence from El Niño and La Niña events. *J. Meteor. Soc. Japan*, **80**, 21–32, https://doi.org/10.2151/jmsj.80.21.

Bell, B., and Coauthors, 2020: ERA5 monthly averaged data on pressure levels from 1950 to 1978 (preliminary version). Copernicus Climate Change Service (C3S) Climate Data Store (CDS), accessed 2 April 2021, https://cds.climate.copernicus.eu/cdsapp#!/dataset/reanalysis-era5-pressure-levels-monthly-means-preliminary-back-extension?tab=overview.

Bird, B. W., M. B. Abbott, M. Vuille, D. T. Rodbell, N. D. Stansell, and M. F. Rosenmeier, 2011: A 2,300-year-long annually resolved record of the South American summer monsoon from the Peruvian Andes. *Proc. Natl. Acad. Sci. USA*, **108**, 8583–8588, https://doi.org/10.1073/pnas.1003719108.

Cai, W., and Coauthors, 2019: Pantropical climate interactions. *Science*, **363**, eaav4236, https://doi.org/10.1126/science.aav4236.

——, and Coauthors, 2020: Climate impacts of the El Niño–Southern Oscillation on South America. *Nat. Rev. Earth Environ.*, **1**, 215–231, https://doi.org/10.1038/s43017-020-0040-3.

Carvalho, L. M. V., C. Jones, and B. Liebmann, 2004: The South Atlantic convergence zone: Intensity, form, persistence, and relationships with intraseasonal to interannual activity and extreme rainfall. *J. Climate*, **17**, 88–108, https://doi.org/10.1175/1520-0442(2004)017<0088:TSACZI>2.0.CO;2.

Chen, Y., and Coauthors, 2011: Forecasting fire season severity in South America using sea surface temperature anomalies. *Science*, **334**, 787–791, https://doi.org/10.1126/science.1209472.

Chylek, P., J. D. Klett, G. Lesins, M. K. Dubey, and N. Hengartner, 2014: The Atlantic Multidecadal Oscillation as a dominant factor of oceanic influence on climate. *Geophys. Res. Lett.*, **41**, 1689–1697, https://doi.org/10.1002/2014GL059274.

Dai, A., 2013: The influence of the inter-decadal Pacific oscillation on U.S. precipitation during 1923-2010. *Climate Dyn.*, **41**, 633–646, https://doi.org/10.1007/s00382-012-1446-5.

——, J. C. Fyfe, S.-P. Xie, and X. Dai, 2015: Decadal modulation of global surface temperature by internal climate variability. *Nat. Climate Change*, **5**, 555–559, https://doi.org/10.1038/nclimate2605.

Day, J. J., J. C. Hargreaves, J. D. Annan, and A. Abe-Ouchi, 2012: Sources of multi-decadal variability in Arctic sea ice extent. *Environ. Res. Lett.*, **7**, 034011, https://doi.org/10.1088/1748-9326/7/3/034011.

Deser, C., A. S. Phillips, and J. W. Hurrell, 2004: Pacific interdecadal climate variability: Linkages between the tropics and the North Pacific during boreal winter since 1900. *J. Climate*, **17**, 3109–3124, https://doi.org/10.1175/1520-0442(2004)017<3109:PICVLB>2.0.CO;2.

Dong, B., and A. Dai, 2015: The influence of the Interdecadal Pacific Oscillation on temperature and precipitation over the globe. *Climate Dyn.*, **45**, 2667–2681, https://doi.org/10.1007/s00382-015-2500-x.

——, and ——, 2017: The uncertainties and causes of the recent changes in global evapotranspiration from 1982 to 2010. *Climate Dyn.*, **49**, 279–296, https://doi.org/10.1007/s00382-016-3342-x.

——, ——, M. Vuille, and O. Elison Timm, 2018: Asymmetric modulation of ENSO teleconnections by the interdecadal Pacific oscillation. *J. Climate*, **31**, 7337–7361, https://doi.org/10.1175/JCLI-D-17-0663.1.

Dong, L., T. Zhou, A. Dai, F. Song, B. Wu, and X. Chen, 2016: The footprint of the Inter-decadal Pacific Oscillation in Indian Ocean sea surface temperatures. *Sci. Rep.*, **6**, 21251, https://doi.org/10.1038/srep21251.

Enfield, D. B., A. M. Mestas-Nuñez, and P. J. Trimble, 2001: The Atlantic Multidecadal Oscillation and its relation to rainfall and river flows in the continental U.S. *Geophys. Res. Lett.*, **28**, 2077–2080, https://doi.org/10.1029/2000GL012745.

England, M. H., and Coauthors, 2014: Recent intensification of wind-driven circulation in the Pacific and the ongoing warming hiatus. *Nat. Climate Change*, **4**, 222–227, https://doi.org/10.1038/nclimate2106.

Figliuolo, G. C., R. V. Andreoli, M. T. Kayano, J. A. C. da Costa, W. H. T. Rego, and D. S. de Moraes, 2020: The role of the Atlantic Multidecadal Oscillation precondition in the teleconnection of different El Niño–Southern Oscillation types and impacts on the 15°N–15°S South American sector precipitation. *Int. J. Climatol.*, **40**, 1943–1964, https://doi.org/10.1002/joc.6309.

Flantua, S. G. A., and Coauthors, 2016: Climate variability and human impact in South America during the last 2000 years: Synthesis and perspectives from pollen records. *Climate Past*, **12**, 483–523, https://doi.org/10.5194/cp-12-483-2016.

Folland, C. K., D. E. Parker, and F. E. Kates, 1984: Worldwide marine temperature fluctuations 1856–1981. *Nature*, **310**, 670–673, https://doi.org/10.1038/310670a0.

Garreaud, R., and D. S. Battisti, 1999: Interannual (ENSO) and Interdecadal (ENSO-like) variability in the Southern Hemisphere tropospheric circulation. *J. Climate*, **12**, 2113–2123, https://doi.org/10.1175/1520-0442(1999)012<2113:IEAIEL>2.0.CO;2.

——, M. Vuille, and A. C. Clement, 2003: The climate of the Altiplano: Observed current conditions and mechanisms of past changes. *Palaeogeogr. Palaeoclimatol. Palaeoecol.*, **194**, 5–22, https://doi.org/10.1016/S0031-0182(03)00269-4.

——, ——, R. Compagnucci, and J. Marengo, 2009: Present-day South American climate. *Palaeogeogr. Palaeoclimatol. Palaeoecol.*, **281**, 180–195, https://doi.org/10.1016/j.palaeo.2007.10.032.

GISTEMP Team, 2020: GISS Surface Temperature Analysis (GISTEMP), version 4. NASA Goddard Institute for Space Studies, accessed 15 May 2020, https://data.giss.nasa.gov/gistemp/.

Harris, I., T. J. Osborn, P. Jones, and D. Lister, 2020: Version 4 of the CRU TS monthly high-resolution gridded multivariate climate dataset. *Sci. Data*, **7**, 109, https://doi.org/10.1038/s41597-020-0453-3.

Hartmann, B., and G. Wendler, 2005: The significance of the 1976 Pacific climate shift in the climatology of Alaska. *J. Climate*, **18**, 4824–4839, https://doi.org/10.1175/JCLI3532.1.

Hastenrath, S., and L. Heller, 1977: Dynamics of climatic hazards in northeast Brazil. *Quart. J. Roy. Meteor. Soc.*, **103**, 77–92, https://doi.org/10.1002/qj.49710343505.

Henley, B. J., J. Gergis, D. J. Karoly, S. Power, J. Kennedy, and C. K. Folland, 2015: A tripole index for the Interdecadal Pacific Oscillation. *Climate Dyn.*, **45**, 3077–3090, https://doi.org/10.1007/s00382-015-2525-1.

Hersbach, H., and Coauthors, 2019: ERA5 monthly averaged data on pressure levels from 1979 to present. Copernicus Climate Change Service (C3S) Climate Data Store (CDS), accessed 2 April 2021, https://doi.org/10.24381/cds.6860a573.

Hua, W., A. Dai, and M. Qin, 2018: Contributions of internal variability and external forcing to the recent Pacific decadal variations. *Geophys. Res. Lett.*, **45**, 7084–7092, https://doi.org/10.1029/2018GL079033.

——, ——, L. Zhou, M. Qin, and H. Chen, 2019: An externally forced decadal rainfall seesaw pattern over the Sahel and southeast Amazon. *Geophys. Res. Lett.*, **46**, 923–932, https://doi.org/10.1029/2018GL081406.

Huang, B., and Coauthors, 2017: NOAA Extended Reconstructed Sea Surface Temperature (ERSST), Version 5. NOAA/National Centers for Environmental Information, accessed 24 June 2020, https://doi.org/10.7289/V5T72FNM.

Huang, D., A. Dai, B. Yang, P. Yan, J. Zhu, and Y. Zhang, 2019: Contributions of different combinations of the IPO and AMO to recent changes in winter East Asian jets. *J. Climate*, **32**, 1607–1626, https://doi.org/10.1175/JCLI-D-18-0218.1.

Ishii, M., A. Shouji, S. Sugimoto, and T. Matsumoto, 2005: Objective analyses of sea-surface temperature and marine meteorological variables for the 20th century using ICOADS and the Kobe Collection. *Int. J. Climatol.*, **25**, 865–879, https://doi.org/10.1002/joc.1169.

Jacques-Coper, M., and R. D. Garreaud, 2015: Characterization of the 1970s climate shift in South America. *Int. J. Climatol.*, **35**, 2164–2179, https://doi.org/10.1002/joc.4120.

Jones, C., 2019: Recent changes in the South America low-level jet. *Climate Atmos. Sci.*, **2**, 20, https://doi.org/10.1038/s41612-019-0077-5.

Kaplan, A., M. A. Cane, Y. Kushnir, A. C. Clement, M. B. Blumenthal, and B. Rajagopalan, 1998: Analyses of global sea surface temperature 1856–1991. *J. Geophys. Res.*, **103**, 18 567–18 589, https://doi.org/10.1029/97JC01736.

Karoly, D. J., 1989: Southern Hemisphere circulation features associated with El Niño–Southern Oscillation events. *J. Climate*, **2**, 1239–1252, https://doi.org/10.1175/1520-0442(1989)002<1239:SHCFAW>2.0.CO;2.

Kayano, M. T., and V. B. Capistrano, 2014: How the Atlantic Multidecadal Oscillation (AMO) modifies the ENSO influence on the South American rainfall. *Int. J. Climatol.*, **34**, 162–178, https://doi.org/10.1002/joc.3674.

——, C. P. de Oliveira, and R. V. Andreoli, 2009: Interannual relations between South American rainfall and tropical sea surface temperature anomalies before and after 1976. *Int. J. Climatol.*, **29**, 1439–1448, https://doi.org/10.1002/joc.1824.

——, R. V. Andreoli, and R. A. F. de Souza, 2011: Evolving anomalous SST patterns leading to ENSO extremes: Relations between the tropical Pacific and Atlantic Oceans and the influence on the South American rainfall. *Int. J. Climatol.*, **31**, 1119–1134, https://doi.org/10.1002/joc.2135.

——, ——, and ——, 2013: Relations between ENSO and the South Atlantic SST modes and their effects on the South American rainfall. *Int. J. Climatol.*, **33**, 2008–2023, https://doi.org/10.1002/joc.3569.

——, ——, and ——, 2019: El Niño–Southern Oscillation related teleconnections over South America under distinct Atlantic Multidecadal Oscillation and Pacific Interdecadal Oscillation backgrounds: La Niña. *Int. J. Climatol.*, **39**, 1359–1372, https://doi.org/10.1002/joc.5886.

——, ——, and ——, 2020: Pacific and Atlantic multidecadal variability relations to the El Niño events and their effects on the South American rainfall. *Int. J. Climatol.*, **40**, 2183–2200, https://doi.org/10.1002/joc.6326.

Kennedy, J. J., N. A. Rayner, R. O. Smith, D. E. Parker, and M. Saunby, 2011a: Reassessing biases and other uncertainties in sea surface temperature observations measured in situ since 1850: 1. Measurement and sampling uncertainties. *J. Geophys. Res.*, **116**, D14103, https://doi.org/10.1029/2010JD015218.

——, ——, ——, ——, and ——, 2011b: Reassessing biases and other uncertainties in sea surface temperature observations measured in situ since 1850: 2. Biases and homogenization. *J. Geophys. Res.*, **116**, D14104, https://doi.org/10.1029/2010JD015220.

Knight, J. R., C. K. Folland, and A. A. Scaife, 2006: Climate impacts of the Atlantic Multidecadal Oscillation. *Geophys. Res. Lett.*, **33**, L17706, https://doi.org/10.1029/2006GL026242.

Krishnan, R., and M. Sugi, 2003: Pacific decadal oscillation and variability of the Indian summer monsoon rainfall. *Climate Dyn.*, **21**, 233–242, https://doi.org/10.1007/s00382-003-0330-8.

Lenssen, N. J. L., G. A. Schmidt, J. E. Hansen, M. J. Menne, A. Persin, R. Ruedy, and D. Zyss, 2019: Improvements in the GISTEMP uncertainty model. *J. Geophys. Res. Atmos.*, **124**, 6307–6326, https://doi.org/10.1029/2018JD029522.

Lenters, J. D., and K. H. Cook, 1997: On the origin of the Bolivian high and related circulation features of the South American climate. *J. Atmos. Sci.*, **54**, 656–678, https://doi.org/10.1175/1520-0469(1997)054<0656:OTOOTB>2.0.CO;2.

Li, X., S.-P. Xie, S. T. Gille, and C. Yoo, 2016: Atlantic-induced pan-tropical climate change over the past three decades. *Nat. Climate Change*, **6**, 275–279, https://doi.org/10.1038/nclimate2840.

Liebmann, B., G. N. Kiladis, J. Marengo, T. Ambrizzi, and J. D. Glick, 1999: Submonthly convective variability over South America and the South Atlantic convergence zone. *J. Climate*, **12**, 1877–1891, https://doi.org/10.1175/1520-0442(1999)012<1877:SCVOSA>2.0.CO;2.

Liu, Z., 2012: Dynamics of interdecadal climate variability: A historical perspective. *J. Climate*, **25**, 1963–1995, https://doi.org/10.1175/2011JCLI3980.1.

Luo, D., Y. Chen, A. Dai, M. Mu, R. Zhang, and I. Simmonds, 2017: Winter Eurasian cooling linked with the Atlantic Multidecadal Oscillation. *Environ. Res. Lett.*, **12**, 125002, https://doi.org/10.1088/1748-9326/aa8de8.

Malhi, Y., J. T. Roberts, R. A. Betts, T. J. Killeen, W. Li, and C. A. Nobre, 2008: Climate change, deforestation, and the fate of the Amazon. *Science*, **319**, 169–172, https://doi.org/10.1126/science.1146961.

Marengo, J. A., and Coauthors, 2008: The drought of Amazonia in 2005. *J. Climate*, **21**, 495–516, https://doi.org/10.1175/2007JCLI1600.1.

Matsuura, K., and C. J. Willmott, 2018a: Terrestrial air temperature: 1900–2017 gridded monthly time series, version 5.01. University of Delaware, accessed 22 April 2020, http://climate.geog.udel.edu/~climate/html_pages/Global2017/README.GlobalTsT2017.html.

——, and ——, 2018b: Terrestrial precipitation: 1900–2017 gridded monthly time series, version 5.01. University of Delaware, accessed 22 April 2020, http://climate.geog.udel.edu/~climate/html_pages/Global2017/README.GlobalTsP2017.html.

Meehl, G. A., and Coauthors, 2021: Atlantic and Pacific tropics connected by mutually interactive decadal-timescale processes. *Nat. Geosci.*, **14**, 36–42, https://doi.org/10.1038/s41561-020-00669-x.

Miles, M. W., D. V. Divine, T. Furevik, E. Jansen, M. Moros, and A. E. J. Ogilvie, 2014: A signal of persistent Atlantic multidecadal variability in Arctic sea ice. *Geophys. Res. Lett.*, **41**, 463–469, https://doi.org/10.1002/2013GL058084.

Mo, K. C., and J. N. Paegle, 2001: The Pacific–South American modes and their downstream effects. *Int. J. Climatol.*, **21**, 1211–1229, https://doi.org/10.1002/joc.685.

Nichols, T. E., and A. P. Holmes, 2002: Nonparametric permutation tests for functional neuroimaging: A primer with examples. *Hum. Brain Mapp.*, **15**, 1–25, https://doi.org/10.1002/hbm.1058.

Nobre, P., and J. Shukla, 1996: Variations of sea surface temperature, wind stress, and rainfall over the tropical Atlantic and South America. *J. Climate*, **9**, 2464–2479, https://doi.org/10.1175/1520-0442(1996)009<2464:VOSSTW>2.0.CO;2.

O'Reilly, C. H., T. Woollings, and L. Zanna, 2017: The dynamical influence of the Atlantic multidecadal oscillation on continental climate. *J. Climate*, **30**, 7213–7230, https://doi.org/10.1175/JCLI-D-16-0345.1.

Power, S., T. Casey, C. Folland, A. Colman, and V. Mehta, 1999: Inter-decadal modulation of the impact of ENSO on Australia. *Climate Dyn.*, **15**, 319–324, https://doi.org/10.1007/s003820050284.

Prado, L. F., I. Wainer, E. Yokoyama, M. Khodri, and J. Garnier, 2021: Changes in summer precipitation variability in central Brazil over the past eight decades. *Int. J. Climatol.*, **41**, 4171–4186, https://doi.org/10.1002/joc.7065.

Qin, M., A. Dai, and W. Hua, 2020a: Quantifying contributions of internal variability and external forcing to Atlantic multidecadal variability since 1870. *Geophys. Res. Lett.*, **47**, e2020GL089504, https://doi.org/10.1029/2020GL089504.

——, ——, and ——, 2020b: Aerosol-forced multidecadal variations across all ocean basins in models and observations since 1920. *Sci. Adv.*, **6**, eabb0425, https://doi.org/10.1126/sciadv.abb0425.

Rayner, N. A., D. E. Parker, E. B. Horton, C. K. Folland, L. V. Alexander, D. P. Rowell, E. C. Kent, and A. Kaplan, 2003: Global analyses of sea surface temperature, sea ice, and night marine air temperature since the late nineteenth century. *J. Geophys. Res.*, **108**, 4407, https://doi.org/10.1029/2002JD002670.

Rojas, M., P. A. Arias, V. Flores-Aqueveque, A. Seth, and M. Vuille, 2016: The South American monsoon variability over the last millennium in climate models. *Climate Past*, **12**, 1681–1691, https://doi.org/10.5194/cp-12-1681-2016.

Ruprich-Robert, Y., R. Msadek, F. Castruccio, S. Yeager, T. Delworth, and G. Danabasoglu, 2017: Assessing the climate impacts of the observed Atlantic multidecadal variability using the GFDL CM2.1 and NCAR CESM1 global coupled models. *J. Climate*, **30**, 2785–2810, https://doi.org/10.1175/JCLI-D-16-0127.1.

——, T. Delworth, R. Msadek, F. Castruccio, S. Yeager, and G. Danabasoglu, 2018: Impacts of the Atlantic multidecadal variability on North American summer climate and heat waves. *J. Climate*, **31**, 3679–3700, https://doi.org/10.1175/JCLI-D-17-0270.1.

Schlesinger, M. E., and N. Ramankutty, 1994: An oscillation in the global climate system of period 65–70 years. *Nature*, **367**, 723–726, https://doi.org/10.1038/367723a0.

Schneider, U., A. Becker, P. Finger, A. Meyer-Christoffer, and M. Ziese, 2018: GPCC full data monthly product version 2018 at 0.5°: Monthly land-surface precipitation from rain-gauges built on GTS-based and historical data. Global Precipitation Climatology Centre, accessed 27 April 2020, https://doi.org/10.5676/DWD_GPCC/FD_M_V2018_050.

Schubert, S., and Coauthors, 2009: A U.S. CLIVAR project to assess and compare the responses of global climate models to drought-related SST forcing patterns: Overview and results. *J. Climate*, **22**, 5251–5272, https://doi.org/10.1175/2009JCLI3060.1.

Slivinski, L. C., and Coauthors, 2019: Towards a more reliable historical reanalysis: Improvements for version 3 of the Twentieth Century Reanalysis System. *Quart. J. Roy. Meteor. Soc.*, **145**, 2876–2908, https://doi.org/10.1002/qj.3598.

Sulca, J., K. Takahashi, J.-C. Espinoza, M. Vuille, and W. Lavado, 2018: Impacts of different ENSO flavors and tropical Pacific convection variability (ITCZ, SPCZ) on austral summer rainfall in South America, with a focus on Peru. *Int. J. Climatol.*, **38**, 420–435, https://doi.org/10.1002/joc.5185.

Sutton, R. T., and B. Dong, 2012: Atlantic Ocean influence on a shift in European climate in the 1990s. *Nat. Geosci.*, **5**, 788–792, https://doi.org/10.1038/ngeo1595.

——, G. D. McCarthy, J. Robson, B. Sinha, A. T. Archibald, and L. J. Gray, 2018: Atlantic multidecadal variability and the U.K. ACSIS program. *Bull. Amer. Meteor. Soc.*, **99**, 415–425, https://doi.org/10.1175/BAMS-D-16-0266.1.

Ting, M., Y. Kushnir, R. Seager, and C. Li, 2009: Forced and internal twentieth-century SST trends in the North Atlantic. *J. Climate*, **22**, 1469–1481, https://doi.org/10.1175/2008JCLI2561.1.

Trenberth, K. E., and D. J. Shea, 2005: Relationships between precipitation and surface temperature. *Geophys. Res. Lett.*, **32**, L14703, https://doi.org/10.1029/2005GL022760.

Vera, C., and Coauthors, 2006: Toward a unified view of the American monsoon systems. *J. Climate*, **19**, 4977–5000, https://doi.org/10.1175/JCLI3896.1.

Villamayor, J., T. Ambrizzi, and E. Mohino, 2018: Influence of decadal sea surface temperature variability on northern Brazil rainfall in CMIP5 simulations. *Climate Dyn.*, **51**, 563–579, https://doi.org/10.1007/s00382-017-3941-1.

Vuille, M., and Coauthors, 2012: A review of the South American monsoon history as recorded in stable isotopic proxies over the past two millennia. *Climate Past*, **8**, 1309–1321, https://doi.org/10.5194/cp-8-1309-2012.

——, E. Franquist, R. Garreaud, W. S. Lavado Casimiro, and B. Cáceres, 2015: Impact of the global warming hiatus on Andean temperature. *J. Geophys. Res. Atmos.*, **120**, 3745–3757, https://doi.org/10.1002/2015JD023126.

Zeng, N., J.-H. Yoon, J. A. Marengo, A. Subramaniam, C. A. Nobre, A. Mariotti, and J. D. Neelin, 2008: Causes and impacts of the 2005 Amazon drought. *Environ. Res. Lett.*, **3**, 014002, https://doi.org/10.1088/1748-9326/3/1/014002.

Zhang, R., and T. L. Delworth, 2006: Impact of Atlantic multidecadal oscillations on India/Sahel rainfall and Atlantic hurricanes. *Geophys. Res. Lett.*, **33**, L17712, https://doi.org/10.1029/2006GL026267.

——, R. Sutton, G. Danabasoglu, Y.-O. Kwon, R. Marsh, S. G. Yeager, D. E. Amrhein, and C. M. Little, 2019: A review of the role of the Atlantic meridional overturning circulation in Atlantic multidecadal variability and associated climate impacts. *Rev. Geophys.*, **57**, 316–375, https://doi.org/10.1029/2019RG000644.

Zhang, Y., J. M. Wallace, and D. S. Battisti, 1997: ENSO-like interdecadal variability: 1900–93. *J. Climate*, **10**, 1004–1020, https://doi.org/10.1175/1520-0442(1997)010<1004:ELIV>2.0.CO;2.

Zilli, M. T., L. M. V. Carvalho, and B. R. Lintner, 2019: The poleward shift of South Atlantic convergence zone in recent decades. *Climate Dyn.*, **52**, 2545–2563, https://doi.org/10.1007/s00382-018-4277-1.